JOURNAL OF PETROLOGY | VOLUME 44 | NUMBER 12 | PAGES 2139–2171 | 2003 | DOI: 10.1093/petrology/egg073

Early Proterozoic Melt Generation Processes beneath the Intra-cratonic Cuddapah Basin, Southern India

M. ANAND[1]*, S. A. GIBSON[1], K. V. SUBBARAO[2], S. P. KELLEY[3] AND A. P. DICKIN[4]

[1]DEPARTMENT OF EARTH SCIENCES, UNIVERSITY OF CAMBRIDGE, CAMBRIDGE CB2 3EQ, UK

[2]DEPARTMENT OF EARTH SCIENCES, INDIAN INSTITUTE OF TECHNOLOGY, MUMBAI, POWAI, 400 076, INDIA

[3]DEPARTMENT OF EARTH SCIENCES, OPEN UNIVERSITY, MILTON KEYNES MK7 6AA, UK

[4]DEPARTMENT OF GEOLOGY, MCMASTER UNIVERSITY, HAMILTON, ONT. L8S 4M1, CANADA

RECEIVED SEPTEMBER 20, 2002; ACCEPTED JUNE 9, 2003

Early Proterozoic tholeiitic lavas and sills were emplaced during the initial phase of extension of the intra-cratonic Cuddapah Basin, southern India. ^{40}Ar–^{39}Ar laser-fusion determinations on phlogopite mica, from the Tadpatri Fm mafic–ultramafic sill complex, constrain the age of the initial phase of extension and volcanism in the basin at 1·9 Ga. Despite their Early Proterozoic age, the igneous rocks are unmetamorphosed, undeformed and remarkably fresh. They exhibit a wide range in MgO contents (4–28 wt %) and have undergone varying degrees of accumulation or crystal fractionation. Variable La/Nb ratios (1·2–3·7) and ε_{Nd} values (1 to −10) suggest that some, but not all, of the mafic rocks have been affected by crustal contamination. This appears to have taken place in magma chambers at ~9 kbar, i.e. the base of the continental crust. Forward modelling of major and trace elements (Fe and Nd) and inverse modelling of rare earth elements suggest that the primary Cuddapah melts were generated by ~10–15% partial melting of a lherzolite mantle source. This corresponds to a mantle potential temperature of ~1500°C. The thickness of the mechanical boundary layer predicted by the geochemical modelling is 70 km with a minimum initial lithospheric thickness of 120 km. This corresponds to a stretching factor of 1·6–1·8. Richter's (1988) secular cooling model for the Earth predicts that, at 1·9 Ga, the ambient mantle had a potential temperature of ~1500°C (i.e. ~200°C hotter than Phanerozoic mantle). If the cooling model is correct then Proterozoic lithospheric stretching and mantle melting beneath the intra-cratonic Cuddapah Basin could have been caused by passive rather than active rifting.

KEY WORDS: *Proterozoic; intra-cratonic; Cuddapah Basin; rare earth element inversion; lithosphere*

INTRODUCTION

Our understanding of the Earth's chemical differentiation, since its formation at 4·5 Ga, has been enhanced by studies of igneous rocks. The discovery of high-MgO volcanic rocks (komatiites), in Archaean greenstone belts, has resulted in a relatively large number of petrological investigations of igneous rocks that formed during the first 2·5 Gyr of the Earth's history. Proterozoic processes are less clearly understood, despite the fact that a relatively large amount of mafic volcanic activity appears to have occurred at this time.

Intra-cratonic basins occur on every major continent and vary in age from Early Archaean to Cenozoic but the mechanism of their formation is not yet fully understood. Nevertheless, their significance in terms of excellent preservation of the Earth's earliest volcanosedimentary records has long been recognized (McKenzie *et al.*, 1980; Bickle & Eriksson, 1982). Some of the Phanerozoic intra-cratonic basins may also be important repositories of hydrocarbon source rocks and hence these basins have been much more intensively studied than their Precambrian counterparts. Prominent intra-cratonic basins on the southern Indian Craton include the Pranhita–Godavari, Chattisgarh and Cuddapah basins. All of these are

*Corresponding author. Present address: Planetary Geosciences Institute, 306 GS Building, University of Tennessee, Knoxville, TN 37996, USA. Telephone: +1-865-974-6024. Fax: +1-865-974-2368. E-mail: anandm@utk.edu

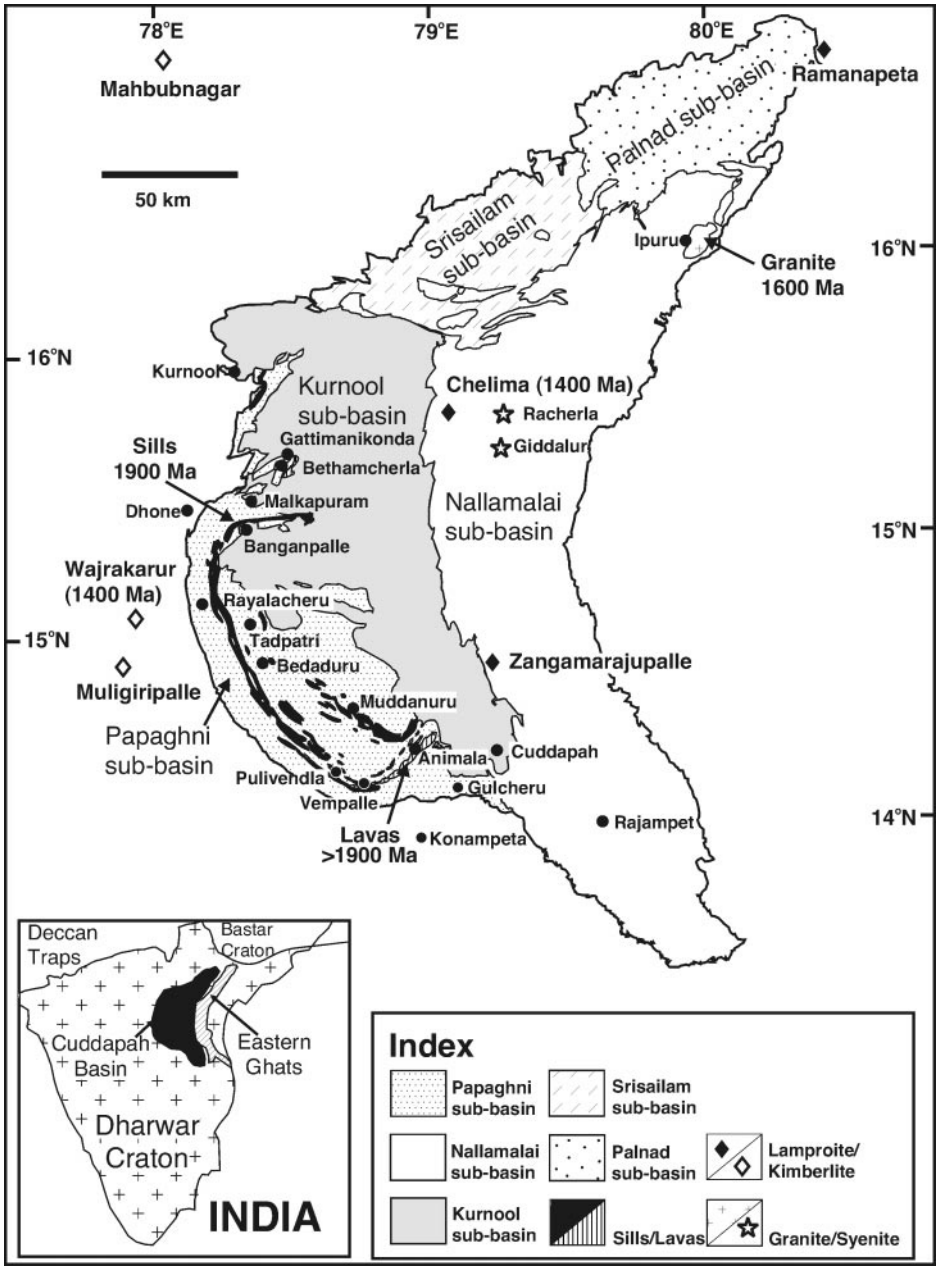

Fig. 1. Geological map of the Cuddapah Basin, after Nagaraja Rao & Ramalingaswamy (1976).

believed to have developed in a rift setting but none of these resulted in continental break-up, although links to an open seaway are evident from the frequent occurrence of deposits representing tidal and storm influence (Chaudhuri *et al.*, 2002). In the present work, the intracratonic Cuddapah Basin has been chosen to study Proterozoic melt generation processes. The basin is believed to have formed ~2·0 Gyr ago and contains a thick (6–12 km), well-preserved, relatively undeformed, volcano-sedimentary succession. Only a few systematic studies have previously been undertaken on the Proterozoic mafic igneous rocks (e.g. Chalapathi Rao, 1997; Chatterjee & Bhattacharji, 1998), which are relatively fresh and suitable for detailed petrological investigations.

GEOLOGY OF THE CUDDAPAH BASIN

The Cuddapah Basin (Fig. 1) is situated in the eastern part of the Dharwar Craton and is one of the largest

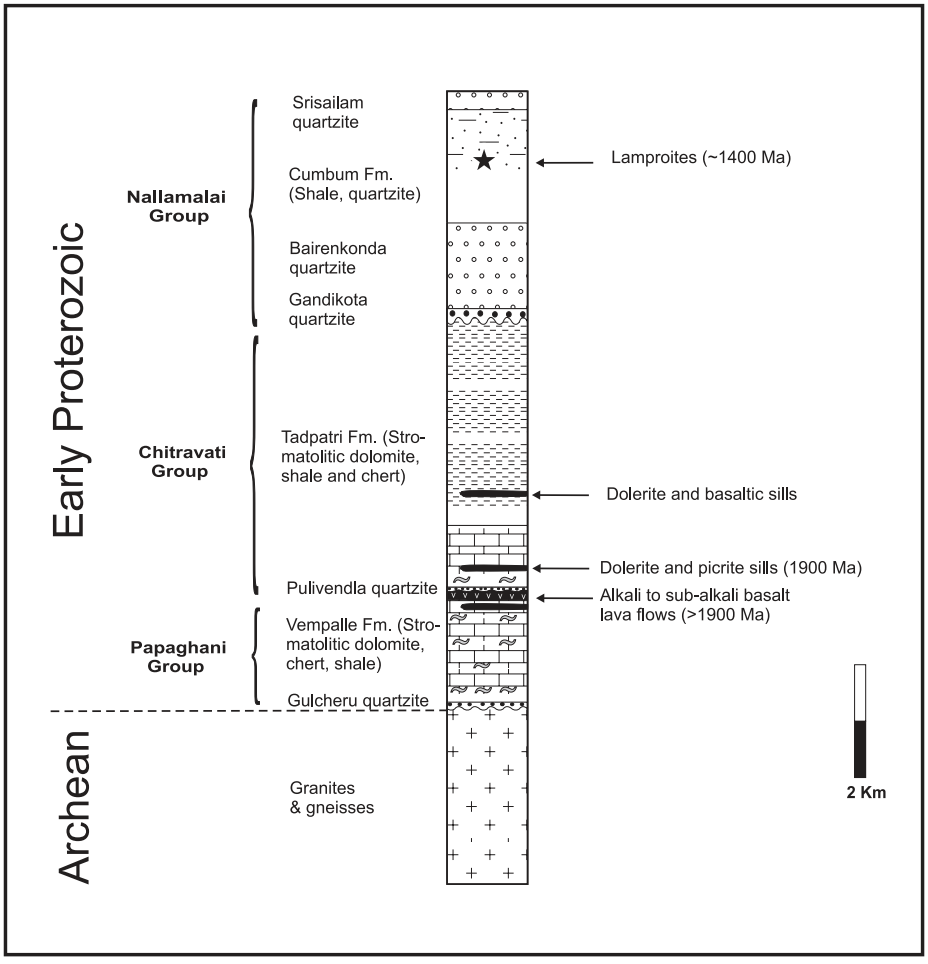

Fig. 2. Stratigraphic column of the Cuddapah Basin.

Proterozoic, intra-cratonic, sedimentary basins in India. It is crescent shaped and covers an area of around 44 500 km^2 with a maximum length and breadth of 440 km and 145 km, respectively. The basin is infilled by a >10 km thick succession of igneous and sedimentary rocks of the Cuddapah and Kurnool Groups (Fig. 2). The western part of the basin has been relatively unaffected by tectonic activity; sedimentary rocks dip gently (10–15°) to the east. In contrast, the eastern part was severely folded and highly metamorphosed during the Middle to Late Proterozoic ($\sim$1·3–1·6 Ga) Eastern Ghat Orogeny (Goodwin, 1996). Extrusive and intrusive mafic volcanic rocks are exposed at lower stratigraphic horizons in the Cuddapah Basin and are mostly subaerial basaltic lavas and sills, occurring in an arcuate pattern, parallel to the margin of the basin (Fig. 1). The present research has therefore mainly focused on the sedimentary and volcanic rocks of the Papaghni sub-basin, situated in the western part of the Cuddapah Basin (Fig. 1). Only those formations in which mafic rocks occur are described in detail below.

Vempalle Formation

The Vempalle Formation is $\sim$1900 m thick (Roy, 1947) and predominantly consists of dolomite with a thin ($\sim$100 m) sandstone–quartzite unit at the base (Fig. 2). It is the only stratigraphic unit that contains a sequence of lava flows. Amygdales occur at the upper surfaces of flows and are usually filled with epidote, calcite and zeolite. The thickest lava flows are recorded in the southern part of the basin at Pulivendla, Vempalle and Animala (up to 50 m). These flows have vesicular tops and appear to be mainly subaerial. At Pulivendla, a basic lava flow conformably overlies the Vempalle Fm dolomites and marks the highest stratigraphic unit of the Papaghni Group.

Lava flows occur in the northern part of the basin at Malkapuram, $\sim$15 km east of Dhone (Fig. 1). Here, hydrothermally altered basaltic lavas form an $\sim$50 m high ridge overlying stromatolitic dolomites and appear to have pillow shapes with chert infillings. The northernmost exposures of lavas in the Cuddapah Basin are at Bethamcherla and Gattimanikonda

Table 1: ^{40}Ar–^{39}Ar laser-fusion data on phlogopite separates from Tadpatri sills

Sample no.	$^{40}Ar/^{39}Ar$	$^{38}Ar/^{39}Ar$	$^{37}Ar/^{39}Ar$	$^{36}Ar/^{39}Ar$	$^{40}Ar^{*}/^{39}Ar$	±	Age (Ma)	±
98MA22 (i)	156·54	0·027	0·33	0·015	152·07	0·32	1854	12
98MA22 (i)	160·70	0·024	0·49	0·018	155·32	0·57	1879	14
98MA22 (i)	161·21	0·022	0·12	0·013	157·30	0·36	1893	12
98MA22 (i)	161·19	0·018	0·23	0·004	160·04	0·32	1914	12
98MA22 (i)	161·34	0·020	0·22	0·001	161·03	0·29	1921	12
98MA22 (i)	162·27	0·019	0·11	0·000	162·27	0·39	1930	12
98MA22 (i)	159·31	0·018	0·19	0·004	157·99	0·20	1899	11
							1899	**20**
98MA78 (ii)	155·65	0·017	0·40	0·000	155·65	0·44	1881	13
98MA78 (ii)	161·68	0·018	0·23	0·000	161·68	0·36	1926	12
98MA78 (ii)	158·11	0·019	0·44	0·001	157·74	0·51	1897	13
98MA78 (ii)	156·86	0·020	0·17	0·000	156·86	0·43	1890	13
							1899	**20**

J value 0·0118 ± 0·000055. Final values shown as 2σ error level weighted means. $^{40}Ar^{*}/^{39}Ar$ is ratio of radiogenic ^{40}Ar to ^{39}Ar produced by irradiation of ^{39}K.

(Fig. 1). These are similar in appearance and composition to the Animala lava flows and reach a total outcrop thickness of ~50–100 m.

Tadpatri Formation

The Tadpatri Formation consists of 4600 m of argillaceous sediments with thin intercalated beds of quartzite and volcanogenic sediments (Fig. 2). The formation is intruded by numerous mafic–ultramafic sills that are exposed at different stratigraphic levels. The thickest (~200 m) sill, which is highly differentiated, extends along the western margin of the Cuddapah Basin for >150 km (Fig. 1) and intrudes stromatolitic dolomites and shales of the lower Tadpatri Formation. Relatively thin (~20 m), single gabbroic and basaltic–doleritic sills occur higher up in the sequence.

Cumbum Formation

Two small (25–30 m in diameter) syenite plugs intrude the Cumbum Formation at Racherla and Giddalur, in the central part of the Cuddapah Basin (Fig. 1). These are resistant to erosion relative to the surrounding Cumbum shales. The syenites are porphyritic with pink phenocrysts (5–10 mm) of K-feldspar set in a fine-grained groundmass. They have clearly undergone extensive hydrothermal alteration. Lamproite dykes intrude the Cumbum Formation at Chelima and Zangamarajupalle (Fig. 1). These are probably contemporaneous with kimberlites that outcrop in the Dharwar Craton (Chalapathi Rao *et al.*, 1999) and Cuddapah Basin syenite intrusions.

AGE AND EMPLACEMENT OF CUDDAPAH IGNEOUS ROCKS

Because of the unfossiliferous nature of the sedimentary rocks from the Cuddapah Basin, its age has mainly been constrained by radiometric dating of igneous rocks. The earliest attempt to determine radiometric ages on Cuddapah rocks was made by Aswathanarayana (1962*a*, 1962*b*) and was followed by a number of workers (e.g. Crawford & Compston, 1973; Murthy *et al.*, 1987; Bhaskar Rao *et al.*, 1995; Chalapathi Rao *et al.*, 1996, 1999). All of these studies have faced problems associated with the low potassium content and alteration of the volcanic samples. Recently, Zachariah *et al.* (1999) used ^{206}Pb–^{204}Pb systematics to date U-mineralized horizons of the Vempalle and Tadpatri Formations. A ^{206}Pb–^{204}Pb age of 1756 ± 29 Ma has been obtained for a U-mineralized sample from the Tadpatri Formation, and has been interpreted as a minimum age for carbonate sedimentation and dolomitization within the Cuddapah Supergroup.

During the present study, ^{40}Ar–^{39}Ar laser-fusion ages were determined for the Tadpatri mafic sills. Electron microprobe analyses were carried out to determine the potassium content of phlogopite crystals. Only samples containing relatively fresh phlogopite crystals were selected for dating. Two sill samples, collected from more than 100 km apart (at Pulivendla and Tadpatri), have given an identical age of 1899 ± 20 Ma (Table 1), which is considered to be their emplacement age. This result is similar to a previously reported Rb–Sr age (1817 ± 24 Ma) for the Pulivendla sill (Bhaskar Rao *et al.*, 1995). Because the sills intrude

the Tadpatri Formation of the Chitravati Group (Fig. 2), the age determination implies that the deposition of the basal volcano-sedimentary sequences in the Cuddapah Basin (the Papaghni and Chitravati Groups) must have occurred prior to ~1900 Ma.

^{40}Ar–^{39}Ar step-heating ages on mica separates from the Chelima lamproite yielded a value of 1417 ± 8·2 Ma (Chalapathi Rao *et al.*, 1999). This dyke intrudes the Cumbum shales of the Nallamalai Group and, as this is the youngest unit of the Cuddapah Supergroup, the emplacement age of the lamproite is considered to be the minimum estimate for the end of the Cuddapah sedimentation.

Many dyke swarms occur at the southern, western and northern margins of the Cuddapah Basin. The majority of them are dolerite but some are amphibolites. These dykes predominantly strike ENE, WNW and north–south. Only one dyke, however, intrudes the Cuddapah sedimentary rocks, near Veldurti (Vijayam, 1968), and hence they are assumed to have been emplaced prior to the formation of the Cuddapah Basin. ^{40}Ar–^{39}Ar and K–Ar ages on mafic dykes from outside the Cuddapah Basin show a large variation from 1879 to 650 Ma (Rao *et al.*, 1995); this wide range in ages could be due to variable argon loss. The oldest ^{40}Ar–^{39}Ar age obtained is 1879 ± 5 Ma for an east–west oriented tholeiitic dyke, adjacent to the southwestern margin of the Cuddapah Basin. This is much younger than the oldest Rb–Sr age of 2420 ± 264 Ma, reported by Ikramuddin & Stueber (1976) for an east–west oriented dyke at Harohalli, near Bangalore.

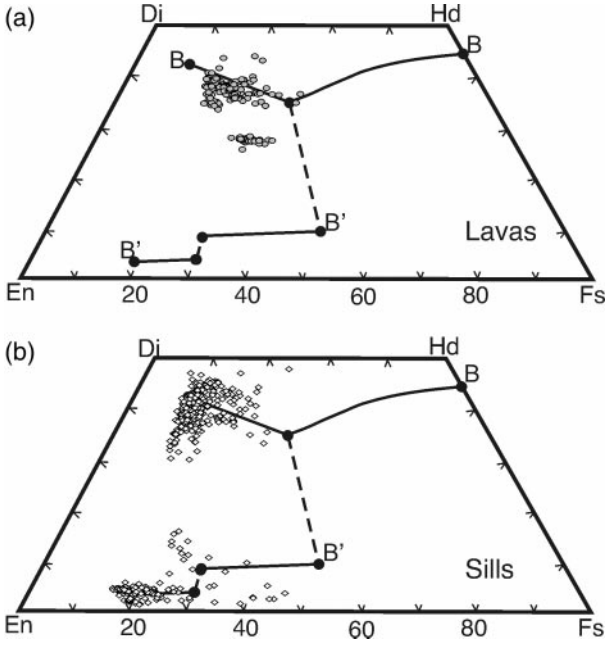

Fig. 3. Pyroxene analyses from Vempalle Fm lavas (a) and Tadpatri sills (b) plotted in the Di–Hd–En–Fs quadrilateral. For simplicity, all Tadpatri sill data have been plotted as one symbol. Fractionation trend of the Skaergaard (BB′) mafic–ultramafic layered intrusions is also shown for comparison. Dashed line is the boundary of the two-pyroxene field.

PETROGRAPHY AND MINERAL CHEMISTRY

Lavas and sills of the Vempalle Formation

Fresh samples of the mafic lavas were difficult to obtain becaue of their susceptibility to weathering and alteration. Feldspars and clinopyroxenes are well preserved in few cases and secondary minerals such as chlorite and white mica are ubiquitous in most samples. Lavas from Bethamcherla contain ~35 modal % of K-rich alkali feldspar phenocrysts and 55 modal % of clinopyroxene along with accessory opaque oxides. All of the other lavas are fine-grained and clinopyroxene is confined to the groundmass. The lack of olivine and presence of iron oxides indicate the fractionated nature of their parental melts. The majority of the pyroxene analyses from the Vempalle Fm lavas form a tight cluster in the augite field of the pyroxene quadrilateral (Fig. 3). Two samples, 98MA07 and 98MA47 (Bethamcherla), are calcium-poor and plot in the subcalcic augite region. The Vempalle Fm lavas exhibit limited variation in feldspar composition; they are dominated by albite-rich ($An_{2–15}$) feldspars together with subordinate amounts of An-rich ($An_{40–60}$) plagioclase (Table 2). Orthoclase-rich feldspars are present in a few samples.

Sills of the Tadpatri Formation

In contrast to the lavas, the coarse-grained mafic–ultramafic sills are relatively fresh; the best exposure is seen near Pulivendla. The base of the sill is marked by a coarse-grained, ultramafic rock; crystals of olivine, pyroxene and, sometimes, phlogopite are easily identifiable in hand specimen. This unit grades upwards into a medium-grained, leucocratic gabbro. Samples from the base of the mafic–ultramafic differentiated sill mainly consist of euhedral to subhedral olivines enclosed by plagioclase feldspar or pyroxene. Modal proportions of ol–opx–cpx–plag vary from 50:30:15:5 to 40:20:20:20. Olivine from this cumulate part of the sill complex is remarkably fresh and has only undergone minor serpentinization along cracks. Crystals are up to 2 mm in length and range in composition from Fo_{78} to Fo_{85}. Spinel grains generally occur at the centre of olivine crystals, implying a co-precipitational origin. The majority of the orthopyroxene analyses plot in the enstatite field and vary from $Ca_2Mg_{80}Fe_{18}$ to $Ca_5Mg_{53}Fe_{42}$ (Fig. 3; Table 2). Orthopyroxene does not occur in the olivine-poor and

Table 2: Representative mineral compositions of the tholeiitic rocks from the Cuddapah Basin

	Lavas				Sills								
					Minor		Major						
	cpx1	cpx2	plag1	plag2	cpx	plag	ol	cpx	pig	opx	plag	phl	sp
Sample no.:	99MA04	98MA07	99MA08	98MA07	98MA92b	98MA92b	98MA97	98MA20	98MA97	99ma55	98MA98	98MA20	98MA39
SiO_2	52·0	51·4	56·2	66·5	50·6	52·6	39·8	53·5	53·5	54·5	49·4	38·1	0·07
TiO_2	0·56	0·38	0·09	0·10	1·16	0·08	—	0·29	0·22	0·13	—	7·45	0·99
Al_2O_3	1·49	4·08	27·4	19·6	2·39	28·6	—	0·47	0·82	0·28	31·3	13·1	11·6
FeO	10·8	16·2	0·73	0·29	11·9	0·82	14·4	7·21	14·9	14·7	0·86	11·6	38·5
MnO	—	—	—	—	—	—	0·21	—	—	—	—	—	0·16
MgO	15·5	13·1	0·09	—	14·8	0·07	44·7	15·2	24·9	27·9	0·10	15·9	5·34
CaO	18·31	11·3	10·2	0·83	17·8	12·3	0·14	22·2	3·80	0·97	14·6	—	—
NiO	—	—	—	—	—	—	0·29	—	—	—	—	—	0·18
Cr_2O_3	—	—	—	—	—	—	0·06	—	—	—	—	—	42·2
Na_2O	0·36	0·8	5·58	11·39	0·47	4·66	—	0·29	0·17	0·04	3·20	0·45	—
K_2O	—	—	0·43	0·15	—	0·24	—	—	—	—	0·17	9·54	—
V_2O_5	—	—	—	—	—	—	—	—	—	—	—	—	0·88
Total	99·5	98·0	100·6	98·8	99·7	99·1	99·6	99·5	98·7	99·0	99·5	96·9	99·9
Mg no.	71·9	59·2			68·9		84·7	78·9	74·9	77·2		71·0	
Wo	37·9	26·7			37·3			45·4	7·6	1·9			
En	44·6	43·3			43·2			43·1	69·2	75·7			
Fs	17·5	29·9			19·5			11·5	23·2	22·4			
An			49·1	3·8		58·4					70·9		
Ab			48·5	95·4		40·2					28·1		

Abbreviations: cpx, clinopyroxene; plag, plagioclase; ol, olivine; pig, pigeonite; opx, orthopyroxene; phl, phlogopite; sp, spinel; —, below detection limit; Mg no. (same as Fo content for olivine) = Mg/(Mg + Fe); Wo (wollastonite) = Ca/(Ca + Mg + Fe); En (enstatite) = Mg/(Ca + Mg + Fe); Fs (ferrosilite) = Fe/(Ca + Mg + Fe); An (anorthite) = Ca/(Ca + Na + K); Ab (albite) = Na/(Ca + Na + K).

highly differentiated portions of the sill or in any other sill or lava sample. Similarly, pigeonite occurs only in samples collected from near the base of the Tadpatri sill complex and varies in composition from $Ca_6Mg_{78}Fe_{16}$ to $Ca_{16}Mg_{63}Fe_{21}$. Augite is by far the dominant Ca-rich pyroxene in the Tadpatri sills and shows a compositional variation from $Ca_{30}Mg_{60}Fe_{10}$ to $Ca_{45}Mg_{35}Fe_{20}$ (Fig. 3; Table 2). In a few cases, clinopyroxene crystals show twinning and hour-glass zoning. Phlogopite forms an accessory phase in the most olivine-rich portions of the sill and appears to have crystallized from inter-cumulus liquid trapped between early-formed olivines.

In the differentiated part of the sill, the olivine is completely serpentinized but the clinopyroxenes are relatively fresh and form large (2–3 mm) sub-ophitic crystals. The pyroxenes have Mg number [Mg/(Mg + Fe) (in mol %)] ranging from 52 to 82. Towards the top of the sill, altered clinopyroxene and plagioclase grains dominate over olivine and orthopyroxene; modal proportions are 40:40:20, respectively. The Tadpatri sills almost exclusively contain plagioclase feldspars. The An content varies from 40 to 80 mol % and the majority of analyses fall in a restricted range between An_{50} and An_{75}, and are labradorites (Table 2). Deer *et al.* (1992) showed that in slow-cooling basic intrusions, such as the Bushveld layered complex, plagioclase feldspar with an An content between 50 and 70% generally crystallizes from inter-cumulus liquid, consistent with the present observations. Granophyres occur in the highly differentiated portions of the sill; they appear to have formed from late-stage fractionated melt. Opaque minerals (ilmenite and magnetite) are fairly common along with plagioclase feldspars and some free quartz.

Many of the small dolerite sills in the upper Tadpatri Formation are characterized by a sub-ophitic texture. The pyroxenes are relatively iron-rich (Table 2) and

plot in the sub-calcic field of the pyroxene quadrilateral. The An content of plagioclase feldspar shows wide variation and range in composition from andesine to labradorite (An_{40-70}).

WHOLE-ROCK GEOCHEMISTRY

Major- and trace-element contents of ~100 samples of igneous rocks from the Cuddapah Basin have been determined to investigate the nature of their parental melts. Representative whole-rock X-ray fluorescence (XRF) and inductively coupled plasma mass spectrometry (ICP-MS) analyses are presented in Table 3.

Hydrothermal alteration and low-grade metamorphism

As a result of their 1·9 Ga age and intense tropical weathering, some of the mafic–ultramafic igneous rocks of the Cuddapah Basin have undergone hydrothermal alteration. The loss-on-ignition (LOI) values for the majority of the Cuddapah lavas and sills range between 1·5 and 3 wt %, but in some rare cases may reach 10 wt %. Only those samples that have LOI values of <3 wt % have been used for detailed geochemical investigations.

Major-element chemistry

On a total alkali vs silica diagram (Fig. 4), the majority of the Cuddapah lava and sill samples plot in the field of subalkaline (tholeiitic) basalts. Exceptions are: (1) the lavas and sills from Bethamcherla and Pulivendla, which plot in the 'trachybasalt' and 'basaltic trachyandesite' fields; (2) the most differentiated Tadpatri samples, which fall in the 'basaltic andesite' field.

In general, the Vempalle Fm lavas and sills show a very restricted range in their SiO_2 (49–52 wt %) and MgO contents (3·6–7·8 wt %). The effects of hydrothermal alteration on the concentrations of highly incompatible elements, such as Na and K, result in wide variation in their bulk-rock contents, as seen in Fig. 5. In some cases, Ca also appears to have been mobilized. Nevertheless, SiO_2, FeO and Al_2O_3 seem to follow a rough fractionation trend when plotted against MgO. The increase in SiO_2 and FeO, and slight decrease in Al_2O_3, with decreasing MgO indicate the involvement of clinopyroxene and feldspar in the fractionating assemblage. In the Vempalle Fm lavas and sills, clinopyroxene and minor plagioclase feldspar fractionation seem to have controlled the evolution of the parental magma (Fig. 5). This is inferred from the lack of correlation between CaO and Al_2O_3 (not shown) and only a moderate decrease in Al_2O_3 content with decreasing MgO.

The majority of the Vempalle Fm lavas and sills are hypersthene (Hy) normative with some of the more evolved samples being quartz (Qtz) normative. Four out of five lava samples from Bethamcherla, one from Vempalle and two sill samples from Pulivendla are nepheline (Ne) normative. This is consistent with their elevated total alkali ($Na_2O + K_2O > 5$ wt %) and relatively high Na_2O contents (>3 wt %). Figure 6 compares the normative compositions of the Vempalle Fm lavas and sills with the results of experimental studies (Thompson *et al.*, 1983). The majority of Vempalle Fm samples plot in an intermediate position between the 1 atm and 9 kbar cotectics. Some of the lavas and sills plot around the experimentally determined dry cotectic for Martindale basalt at 3·5 kbar (Helz, 1980), which suggests that they were derived from parental melts that had undergone significant fractionation at a depth of 10–15 km (3–5 kbar) prior to emplacement.

In contrast to the Vempalle Fm lavas and sills, the sills from the Tadpatri Formation show a large variation in silica (~44–52 wt %) and MgO contents (4–28 wt %) and follow an apparent fractionation trend in Fig. 5. The mafic–ultramafic sills from the Tadpatri Formation have been subdivided into: (1) 'major' sills that occur near the base of the Tadpatri Fm as a large differentiated sill complex, extending over 150 km along the western margin of the Papaghni sub-basin (Fig. 1)—samples from these have been further subdivided into 'cumulate' (≥10 wt % MgO) and 'differentiated' sills (<10 wt % MgO); (2) 'minor' sills—these are further subdivided into 'doleritic' and 'basaltic' sills, occurring at various stratigraphic levels in the Tadpatri Formation. The 'minor' basaltic sills are spatially related to the northernmost outcrop of the differentiated sill complex near Banganpalle.

The effect of hydrothermal alteration is minimal in these rocks, as evident by their low LOI (1–3 wt %) and the strong correlation between major-element oxides (e.g. Na_2O and CaO) and MgO content (Fig. 5). The 'cumulate' samples show an increase in all the major-element oxide concentrations, except for FeO^*, with decreasing MgO consistent with olivine fractionation (Fig. 5). Samples from the 'differentiated' gabbroic parts of the sill, on the other hand, show a sharp decrease in FeO^* and an abrupt increase in Al_2O_3 and CaO concentrations with decreasing MgO content, possibly as a result of orthopyroxene fractionation.

The majority of the Tadpatri sills are Hy-normative but some of the SiO_2-rich (50–52 wt %) samples are Qtz-normative. One sill sample is Ne-normative, probably because of its relatively high Na_2O content (2·7 wt %). Some of the Tadpatri sill samples plot along the 9 kbar cotectic in Fig. 6; exceptions are the MgO-rich samples that form a trend towards the

Table 3: Major-, trace- and rare earth element analyses for Cuddapah Basin samples

Sample:	98MA07	98MA47	98MA49	99MA04	99MA74	99MA76	99MA80	99MA81	99MA08	98MA73
Rock type:	Basalt	Basalt	Basalt	Basalt	Basalt	Basalt	Bas flow1	Bas flow2	Basalt	Basalt
Location:	Beth	Beth	Beth	Gat	Gat	Gat	Gat	Gat	Golapalle	Ranga
Unit:	Vem Fm	Vem Fm	Vem Fm	Vem Fm	Vem Fm	Vem Fm	Vem Fm	Vem Fm	Vem Fm	
Age (Ma):	>1900	>1900	>1900	>1900	>1900	>1900	>1900	>1900	>1900	>1900
wt %										
SiO_2	52·01	49·54	50·96	50·09	51·11	52·12	50·91	50·01	51·56	49·72
TiO_2	1·78	1·86	1·90	1·14	1·33	1·47	1·31	1·29	1·40	1·29
Al_2O_3	13·42	13·84	14·30	15·66	15·42	13·83	13·69	14·08	14·22	14·46
Fe_2O_3	14·76	17·65	16·46	13·18	14·07	14·08	14·35	14·49	13·10	14·74
FeO*	13·28	15·88	14·81	11·86	12·66	12·67	12·91	13·04	11·79	13·26
MnO	0·17	0·19	0·20	0·18	0·18	0·18	0·21	0·21	0·21	0·20
MgO	5·72	6·31	5·87	6·48	5·43	5·52	5·91	6·71	6·15	6·89
CaO	5·11	4·85	5·72	10·21	8·90	9·25	9·15	9·63	7·61	8·79
Na_2O	5·35	4·91	4·61	2·88	2·15	2·32	2·80	2·54	1·93	2·57
K_2O	0·49	1·20	1·07	0·26	1·47	1·05	1·08	0·71	2·96	0·82
P_2O_5	0·25	0·27	0·28	0·13	0·17	0·19	0·15	0·14	0·15	0·15
Total	99·06	100·62	101·37	100·22	100·23	100·00	99·56	99·81	99·29	99·63
LOI	1·57	1·86	1·75	3·47	2·77	2·13	2·07	1·45	1·82	2·17
Mg no.	52·37	50·36	50·29	58·25	52·27	52·66	55·05	56·78	57·12	57·01
ppm										
Ba	317	1340	1243	120	627	304	324	223	846	299
Co	42·2	53·7	60·9	47·7	46·9	52·9	51·9	55·1	46·3	61
Cr	102	103	106	177	101	121	256	149	130	153
Cu	28·5	93·7	55·5	146·7	130·2	143·4	84·5	136·6	146·2	116·2
Ga	7·1	6·4	10·3	12·8	13·5	14·7	14·3	15·1	15·1	11·7
Hf	4·25	4·26	4·45	2·50	2·76	2·48	2·63	2·84	2·99	2·59
Nb	9·78	9·71	10·33	5·31	4·37	4·06	6·28	5·24	6·85	5·41
Ni	67	69	75	81	104	61	69	103	69	111
Pb	2·05	1·57	1·82	4·35	4·17	5·68	5·68	4·60	6·71	3·54
Rb	8·0	26·0	24·6	7·3	31·6	29·9	30·0	20·4	46·3	20·2
Sc	41·7	40·2	41·6	38·2	37·0	36·0	36·0	41·1	39·9	45·2
Sr	111·8	135·0	176	218	262	184	200	186	142·9	191
Ta	0·86	0·94	1·16	0·71	0·48	0·44	0·73	0·47	0·64	0·68
Th	5·85	5·60	5·95	3·63	3·81	3·23	4·34	2·66	4·96	2·59
U	1·62	1·46	1·50	1·04	0·83	0·73	1·27	0·65	1·45	0·67
V	260	280	299	206	137	234	192	199	233	230
Y	33·73	33·00	33·40	21·03	23·87	21·47	22·33	23·83	23·63	23·47
Zn	91·4	111·3	117·5	82·7	90·9	94·3	110·6	107·1	87·2	95·9
Zr	148·0	141·7	150·3	79·9	86·4	80·5	87·7	90·6	102·3	87·3
La	12·53	22·10	20·67	11·60	11·97	10·47	12·80	11·10	13·97	10·33
Ce	31·07	47·67	45·00	25·87	25·17	22·57	28·43	24·17	29·33	24·43
Pr	4·35	5·69	5·42	3·11	3·04	2·67	3·41	3·11	3·77	2·90
Nd	20·37	23·50	22·00	13·57	12·83	11·57	14·13	13·80	15·53	12·83
Sm	5·64	5·62	5·53	3·26	3·47	3·04	3·47	3·46	3·86	3·36
Eu	1·75	2·08	1·92	1·28	1·17	1·10	1·33	1·40	1·53	1·37
Gd	6·64	7·61	7·33	4·12	4·25	4·01	4·78	4·51	5·39	4·50
Tb	1·13	1·09	1·07	0·68	0·75	0·64	0·70	0·76	0·79	0·70

Sample:	98MA07	98MA47	98MA49	99MA04	99MA74	99MA76	99MA80	99MA81	99MA08	98MA73
Rock type:	Basalt	Basalt	Basalt	Basalt	Basalt	Basalt	Bas flow1	Bas flow2	Basalt	Basalt
Location:	Beth	Beth	Beth	Gat	Gat	Gat	Gat	Gat	Golapalle	Ranga
Unit:	Vem Fm	Vem Fm	Vem Fm	Vem Fm	Vem Fm	Vem Fm	Vem Fm	Vem Fm	Vem Fm	
Age (Ma):	>1900	>1900	>1900	>1900	>1900	>1900	>1900	>1900	>1900	>1900
Dy	6·99	6·64	6·76	4·32	4·90	4·13	4·64	4·91	4·92	4·49
Ho	1·44	1·37	1·38	0·84	0·99	0·92	0·86	0·98	0·99	0·97
Er	4·40	4·05	4·07	2·57	3·12	2·74	2·59	2·82	3·03	2·77
Tm	0·60	0·58	0·59	0·35	0·44	0·38	0·35	0·41	0·40	0·38
Yb	3·91	3·65	3·81	2·39	2·84	2·59	2·70	2·84	2·85	2·57
Lu	0·53	0·55	0·56	0·35	0·41	0·38	0·34	0·38	0·43	0·36

Sample:	99MA34	99MA36	99MA37	99MA27	99MA53	99MA86	98MA103	98MA10	98MA74	98MA76
Rock type:	Bas flow1	Bas flow3	Bas flow3	Basalt	Basalt	Basalt	Dol sill	Dolerite	Dol sill	Bas sill
Location:	Animala	Animala	Animala	Vem	Vemula	Brah	Kal Mines	Kur-Beth	Krish	Krish
Unit:	Vem Fm	Vem Fm	Vem Fm	Vem Fm	Vem Fm	Vem Fm	Vem Fm		Tad Fm	Tad Fm
Age (Ma):	>1900	>1900	>1900	>1900	>1900	>1900			1900	1900
Sill type:									Minor (bas sill)	Minor (bas sill)
wt %										
SiO_2	49·40	49·79	51·05	50·72	50·26	51·81	51·16	50·23	49·61	49·21
TiO_2	1·03	1·21	1·09	1·22	1·23	1·81	1·68	1·05	1·05	0·97
Al_2O_3	15·05	15·46	14·69	15·61	15·83	12·76	12·93	14·22	14·39	14·83
Fe_2O_3	13·38	13·55	12·50	13·34	13·78	17·72	16·76	15·23	15·22	14·29
FeO*	12·04	12·19	11·25	12·00	12·40	15·94	15·08	13·70	13·70	12·86
MnO	0·22	0·19	0·18	0·19	0·23	0·20	0·21	0·20	0·20	0·19
MgO	7·78	5·65	7·12	5·54	6·14	3·84	5·74	7·60	6·90	7·48
CaO	8·73	9·40	9·22	9·17	7·41	5·20	7·41	8·93	9·39	9·44
Na_2O	2·35	2·31	2·75	2·35	3·21	1·30	3·86	2·07	2·15	1·98
K_2O	1·62	1·59	1·33	1·89	2·08	4·32	0·91	1·23	0·60	0·80
P_2O_5	0·11	0·14	0·13	0·14	0·13	0·24	0·23	0·12	0·12	0·10
Total	99·67	99·29	100·06	100·17	100·29	99·21	100·90	100·88	99·63	99·29
LOI	2·64	1·90	2·38	1·76	2·38	5·11	2·29	1·86	1·76	1·99
Mg no.	62·26	54·19	61·78	54·09	55·83	38·07	49·28	58·61	56·26	59·76
ppm										
Ba	277	445	263	491	909	1290	284	355	178	207
Co	56	47	54·8	43·9	48·7	42·2	59·9	66·9	70·7	62·4
Cr	265	189	168	107	103	17	63	100	80	118
Cu	59·8	101·3	70·2	89·5	11·7	140·9	94·3	76·6	72·9	66·5
Ga	14·0	15·4	15·8	14·2	14·4	12·2	8·4	10·7	6·6	10·4
Hf	1·69	2·41	2·44	2·45	2·51	3·98	4·00	2·69	3·70	3·36
Nb	4·20	5·91	5·41	5·74	5·75	10·60	8·81	4·44	8·49	8·47
Ni	107	82	89	69	61	14	65	166	154	157
Pb	2·87	4·38	5·58	4·75	5·32	15·30	2·24	4·27	30·57	4·22
Rb	34·7	38·6	37·3	51·7	49·7	85·7	14·5	37·6	17·0	23·9
Sc	38·7	34·8	33·8	34·1	35·8	39·5	43·7	38·0	32·9	38·1
Sr	155	160	216	181	143·2	242	154	152	145·0	143·2
Ta	0·94	0·91	0·80	1·17	0·65	0·83	0·72	0·48	0·80	0·80

Table 3: continued

Sample:	99MA34	99MA36	99MA37	99MA27	99MA53	99MA86	98MA103	98MA10	98MA74	98MA76
Rock type:	Bas flow1	Bas flow3	Bas flow3	Basalt	Basalt	Basalt	Dol sill	Dolerite	Dol sill	Bas sill
Location:	Animala	Animala	Animala	Vem	Vemula	Brah	Kal Mines	Kur-Beth	Krish	Krish
Unit:	Vem Fm	Vem Fm	Vem Fm	Vem Fm	Vem Fm	Vem Fm	Vem Fm		Tad Fm	Tad Fm
Age (Ma):	>1900	>1900	>1900	>1900	>1900	>1900			1900	1900
Sill type:									Minor (bas sill)	Minor (bas sill)
Th	1·73	3·57	4·80	3·63	3·89	9·04	5·06	3·72	5·76	6·17
U	0·32	1·03	1·19	1·03	0·98	2·84	1·24	0·81	0·84	1·56
V	192	196	205	209	191	245	260	231	227	224
Y	17·40	20·17	18·07	19·90	20·60	30·63	32·03	24·37	25·77	24·27
Zn	102·2	114·2	92·7	98·4	116·3	100·5	109·9	103·5	84·4	93·7
Zr	52·1	81·6	82·3	79·7	82·8	140·7	131·3	86·9	129·0	117·7
La	6·99	11·07	12·60	11·00	11·40	21·93	16·83	11·70	21·87	17·43
Ce	18·07	24·87	28·20	24·50	25·90	45·83	36·20	24·90	44·70	38·13
Pr	2·09	2·98	3·29	2·84	2·99	5·35	4·70	2·88	5·02	4·51
Nd	9·43	12·70	13·63	12·23	12·33	22·00	20·30	12·53	20·37	18·33
Sm	2·42	3·04	3·13	3·01	3·14	5·27	5·25	3·23	4·80	4·43
Eu	1·00	1·28	1·24	1·27	1·38	2·03	1·43	1·19	1·81	1·54
Gd	3·26	4·17	3·87	4·26	4·57	6·95	6·18	4·64	6·16	5·30
Tb	0·52	0·64	0·58	0·63	0·66	1·02	1·03	0·78	0·83	0·84
Dy	3·42	4·11	3·77	3·86	4·22	6·06	6·60	4·76	5·03	4·77
Ho	0·74	0·89	0·76	0·79	0·87	1·30	1·38	1·02	1·07	1·01
Er	2·21	2·39	2·20	2·35	2·56	3·71	4·16	3·08	3·09	2·93
Tm	0·28	0·35	0·30	0·33	0·35	0·55	0·61	0·46	0·42	0·43
Yb	1·75	2·40	2·09	2·10	2·41	3·57	3·62	2·85	2·80	2·68
Lu	0·26	0·33	0·30	0·31	0·33	0·50	0·55	0·47	0·42	0·38

Sample:	98MA77	98MA78	98MA79	98MA80	98MA81	99MA23	99MA21	98MA83	98MA84	98MA93
Rock type:	Bas sill	Picrite sill	Dol sill	Dol sill	Bas sill	Picrite sill	Picrite sill	Bas sill	Bas sill	Dol sill
Location:	Krish	Quarry	Quarry	Quarry	Quarry	Quarry	Rayalacheru	Well, Kond	Well, Kond	Bedaduru
Unit:	Tad Fm	Tad Fm	Tad Fm	Tad Fm	Tad Fm	Tad Fm	Tad Fm	Tad Fm	Tad Fm	
Age (Ma):	1900	1900	1900	1900	1900	1900	1900	1900	1900	
Sill type:	Minor (bas sill)	Major (cum)	Major (dif)	Major (dif)	Major (cum)	Major (cum)	Major (cum)	Minor (dol sill)	Minor (dol sill)	Minor (dol sill)
wt %										
SiO_2	50·91	47·68	52·38	52·03	49·91	46·49	46·19	52·23	50·96	47·52
TiO_2	1·22	0·44	0·53	0·53	0·62	0·39	0·30	1·63	1·38	1·78
Al_2O_3	13·56	9·60	15·58	15·95	13·21	8·34	8·14	12·63	13·89	15·32
Fe_2O_3	15·87	12·81	9·08	9·14	11·13	13·22	13·20	16·43	15·57	14·78
FeO*	14·28	11·53	8·17	8·22	10·01	11·90	11·88	14·78	14·01	13·30
MnO	0·26	0·18	0·15	0·15	0·16	0·19	0·18	0·21	0·18	0·19
MgO	5·68	20·24	7·59	8·36	10·93	24·18	25·58	4·24	4·94	6·70
CaO	9·57	7·13	11·33	10·49	10·71	6·15	5·94	7·51	7·84	9·98
Na_2O	2·00	0·86	1·89	1·80	1·16	0·65	0·48	2·94	2·77	2·22

Sample:	98MA77	98MA78	98MA79	98MA80	98MA81	99MA23	99MA21	98MA83	98MA84	98MA93
Rock type:	Bas sill	Picrite sill	Dol sill	Dol sill	Bas sill	Picrite sill	Picrite sill	Bas sill	Bas sill	Dol sill
Location:	Krish	Quarry	Quarry	Quarry	Quarry	Quarry	Rayalacheru	Well, Kond	Well, Kond	Bedaduru
Unit:	Tad Fm	Tad Fm	Tad Fm	Tad Fm	Tad Fm	Tad Fm	Tad Fm	Tad Fm	Tad Fm	
Age (Ma):	1900	1900	1900	1900	1900	1900	1900	1900	1900	
Sill type:	Minor (bas sill)	Major (cum)	Major (dif)	Major (dif)	Major (cum)	Major (cum)	Major (cum)	Minor (dol sill)	Minor (dol sill)	Minor (dol sill)
K_2O	0·17	0·25	0·50	0·52	0·10	0·33	0·42	1·81	1·15	0·39
P_2O_5	0·13	0·06	0·06	0·06	0·08	0·05	0·04	0·38	0·31	0·21
Total	99·37	99·25	99·10	99·04	98·01	99·98	100·48	100·01	98·99	99·08
LOI	2·10	2·74	1·97	2·26	4·89	3·73	4·11	1·04	1·60	2·05
Mg no.	50·38	81·76	70·34	72·18	73·59	83·84	84·61	42·27	47·37	56·26
ppm										
Ba	70	114	156	171	49	78	78	524	296	141
Co	62·2	97·5	33·8	40·5	57·2	108·6	110·8	51·9	52·3	58·2
Cr	99	1996	461	677	1129	2641	2872	87	86	273
Cu	93·7	60·1	101·2	85·6	85·4	51·2	43·8	54·5	50·3	110·2
Ga	12·3	6·0	14·8	16·7	12·1	11·2	10·7	18·2	12·1	9·3
Hf	2·79	1·34	1·52	1·36	1·71	1·27	1·08	3·86	3·25	3·39
Nb	5·23	2·25	2·79	2·55	2·89	1·99	1·51	6·35	5·38	4·72
Ni	95	706	86	97	353	824	900	34	57	149
Pb	8·50	3·57	3·93	3·83	8·77	3·65	2·48	13·43	7·34	4·06
Rb	2·7	13·6	14·0	17·7	3·0	19·3	18·5	46·2	28·2	11·5
Sc	42·8	28·8	39·0	31·6	35·6	27·2	25·2	40·3	35·5	34·5
Sr	93·8	79·1	172	214	74·1	61·6	60·0	246	239	222
Ta	0·62	0·47	0·48	0·44	0·41	0·79	0·87	0·53	0·46	0·52
Th	4·26	3·17	3·80	3·18	3·99	2·79	1·94	3·21	2·79	1·47
U	0·91	0·62	0·74	0·67	0·75	0·56	0·37	0·42	0·38	0·26
V	279	157	215	199	220	104	84	244	220	240
Y	27·20	11·07	13·60	11·63	14·93	9·46	6·93	30·57	25·73	26·13
Zn	108·4	66·0	59·8	53·5	80·6	79·3	75·1	210·4	103·3	85·9
Zr	90·4	41·5	51·1	43·5	56·2	35·5	25·0	136·3	115·0	120·3
La	13·10	8·11	9·53	8·07	10·83	6·81	4·98	24·20	20·43	11·37
Ce	28·83	17·83	21·10	18·17	21·40	16·57	13·13	51·03	43·23	28·00
Pr	3·33	1·81	2·15	1·90	2·38	1·53	1·11	6·00	5·00	3·55
Nd	13·70	7·13	8·58	7·25	9·30	5·97	4·39	25·00	20·70	16·17
Sm	3·48	1·63	1·98	1·60	1·97	1·38	0·98	5·21	4·57	4·30
Eu	1·21	0·50	0·74	0·62	0·76	0·49	0·37	1·83	1·56	1·62
Gd	4·59	2·08	2·60	2·18	2·69	1·78	1·34	6·27	5·37	5·35
Tb	0·82	0·32	0·40	0·33	0·47	0·28	0·21	0·95	0·82	0·89
Dy	5·29	2·10	2·52	2·12	2·83	1·86	1·36	5·81	4·78	5·26
Ho	1·15	0·46	0·54	0·46	0·62	0·38	0·29	1·24	1·03	1·13
Er	3·45	1·30	1·62	1·47	1·93	1·19	0·91	3·80	3·21	3·15
Tm	0·47	0·21	0·24	0·21	0·26	0·16	0·13	0·54	0·44	0·41
Yb	3·10	1·27	1·56	1·38	1·74	1·20	0·94	3·62	3·01	2·78
Lu	0·48	0·18	0·25	0·23	0·24	0·15	0·12	0·52	0·46	0·38

Table 3: continued

Sample:	99MA40	98MA92a	98MA21	98MA22	98MA24	98MA94	98MA19bo	98MA20bo	98MA96	98MA97bo
Rock type:	Dol sill	Dol sill	Picrite sill	Picrite sill	Dol sill	Dol sill	Picrite sill	Pic sill base	Dol sill	Picrite sill
Location:	Mudd	Pul-Mudd	Velpula	Vemula	Vemula	Yer-Vem	Pul-DC	Pul-DC	Pul-DC	R/S Pul-DC
Unit:	Tad Fm	Tad Fm	Tad Fm	Tad Fm	Tad Fm	Tad Fm	Tad Fm	Tad Fm	Tad Fm	Tad Fm
Age (Ma):			1900	1900	1900	1900	1900 Ma	1900	1900	1900
Sill type:	Minor (dol sill)	Minor (dol sill)	Major (cum)	Major (cum)	Major (dif)	Minor (dol sill)	Major (cum)	Major (cum)	Major (dif)	Major (cum)
wt %										
SiO_2	51·17	52·06	44·69	47·42	51·85	47·02	44·48	48·55	51·43	50·63
TiO_2	2·16	1·50	0·30	0·45	0·46	1·59	0·23	0·51	0·41	0·57
Al_2O_3	13·15	13·25	6·87	9·65	17·55	15·05	7·17	10·69	16·55	11·90
Fe_2O_3	15·88	16·79	13·67	12·60	8·22	15·08	13·60	12·42	8·49	12·01
FeO*	14·29	15·11	12·30	11·34	7·40	13·57	12·24	11·18	7·64	10·81
MnO	0·22	0·22	0·19	0·18	0·14	0·20	0·18	0·18	0·14	0·18
MgO	4·98	3·91	27·19	20·12	9·02	7·32	27·63	17·25	9·41	15·40
CaO	8·44	6·87	5·21	7·25	10·78	10·08	5·32	8·28	10·27	9·03
Na_2O	2·52	2·68	0·56	0·82	1·77	1·90	0·50	1·03	1·64	1·28
K_2O	0·82	2·45	0·31	0·47	0·83	0·59	0·25	0·39	0·62	0·43
P_2O_5	0·25	0·37	0·04	0·06	0·06	0·17	0·03	0·06	0·05	0·08
Total	99·58	100·09	99·03	99·01	100·67	99·00	99·40	99·36	99·02	101·51
LOI	2·57	0·98	3·04	2·58	2·37	2·48	2·80	2·24	1·87	2·23
Mg no.	47·08	39·79	84·95	81·92	75·69	57·93	85·22	79·76	75·87	78·44
ppm										
Ba	197	631	65	111	207	182	56	128	181	152
Co	50·2	55	116	83·5	28·9	68·3	115·5	76·2	38·8	74·9
Cr	65	52	3102	2087	754	225	3087	1719	881	1318
Cu	120·4	48·9	41·2	60·7	61·2	176	39·7	64·6	74·1	73·8
Ga	14·4	14·0	n.d.	5·0	12·6	13·4	3·2	6·3	15·9	4·8
Hf	4·54	3·51	1·16	1·56	1·49	2·78	0·61	1·33	1·11	1·38
Nb	7·48	6·55	1·73	2·36	3·09	4·03	0·95	2·33	2·18	2·43
Ni	47	28	1008	677	71	177	1021	559	103	467
Pb	11·23	22·77	2·53	3·01	2·72	2·74	2·26	3·95	2·50	3·81
Rb	25·6	53·6	11·4	17·0	23·4	14·0	12·5	15·6	22·9	18·3
Sc	43·4	36·4	24·1	29·8	30·1	37·1	20·1	28·9	30·8	31·1
Sr	154	249	56·7	83·7	126·3	308	60·3	92·5	134·9	88·5
Ta	0·83	0·50	1·21	0·80	1·86	0·44	0·17	0·22	0·34	0·25
Th	5·82	3·27	2·19	3·17	3·11	0·93	1·05	3·10	2·89	3·40
U	1·16	0·46	0·37	0·62	0·53	0·20	0·20	0·61	0·56	0·57
V	269	226	116	168	181	241	111	179	175	193
Y	34·67	29·27	7·14	10·90	10·77	24·97	5·16	12·20	10·13	13·20
Zn	121·3	163·7	70·1	55·7	53·0	104·0	63·9	67·3	56·1	58·3
Zr	157·7	127·3	24·4	43·1	42·8	95·5	16·3	42·8	38·2	46·5
La	18·03	24·33	5·08	7·79	7·95	7·78	3·29	8·06	7·20	9·10
Ce	40·80	50·47	13·70	18·00	18·17	21·43	6·59	16·13	17·00	18·17
Pr	5·13	6·10	1·13	1·75	1·76	2·73	0·75	1·79	1·68	2·11
Nd	22·47	25·43	4·48	6·81	6·46	13·27	2·99	6·72	6·64	8·44
Sm	5·48	5·16	1·00	1·51	1·57	3·91	0·68	1·72	1·51	2·00
Eu	1·97	1·88	0·35	0·55	0·61	1·52	0·29	0·63	0·60	0·66
Gd	6·92	6·34	1·30	2·04	2·04	4·81	0·95	2·11	1·98	2·57

Sample:	99MA40	98MA92a	98MA21	98MA22	98MA24	98MA94	98MA19bo	98MA20bo	98MA96	98MA97bo
Rock type:	Dol sill	Dol sill	Picrite sill	Picrite sill	Dol sill	Dol sill	Picrite sill	Pic sill base	Dol sill	Picrite sill
Location:	Mudd	Pul-Mudd	Velpula	Vemula	Vemula	Yer-Vem	Pul-DC	Pul-DC	Pul-DC	R/S Pul-DC
Unit:	Tad Fm	Tad Fm	Tad Fm	Tad Fm	Tad Fm	Tad Fm	Tad Fm	Tad Fm	Tad Fm	Tad Fm
Age (Ma):			1900	1900	1900	1900	1900 Ma	1900	1900	1900
Sill type:	Minor (dol sill)	Minor (dol sill)	Major (cum)	Major (cum)	Major (dif)	Minor (dol sill)	Major (cum)	Major (cum)	Major (dif)	Major (cum)
Tb	1·11	0·89	0·20	0·32	0·31	0·84	0·15	0·35	0·32	0·35
Dy	7·00	5·38	1·43	2·11	1·98	5·13	1·03	2·17	1·85	2·45
Ho	1·42	1·19	0·28	0·45	0·42	1·01	0·19	0·50	0·42	0·57
Er	4·01	3·61	0·94	1·31	1·35	3·01	0·70	1·40	1·26	1·60
Tm	0·58	0·51	0·12	0·20	0·20	0·40	0·09	0·22	0·17	0·20
Yb	3·79	3·47	0·89	1·38	1·21	2·66	0·57	1·37	1·17	1·56
Lu	0·53	0·51	0·12	0·18	0·19	0·35	0·09	0·21	0·20	0·24

Sample:	98MA98	99MA55	99MA56	99MA50	98MA114	99MA60	98MA03	99MA63	98MA119bo	98MA123
Rock type:	Picrite sill	Picrite sill	Dol sill	Dol dyke	Dol dyke	Dol dyke	Granite	Granite	Kimberlite	Kimberlite
Location:	R/S Pul-DC	Pul-DC	Pul-DC	Anj	Kon	Mir	Kur	Ipuru	Mul	Mul
Unit:	Tad Fm	Tad Fm	Tad Fm	Bmt	Bmt	Bmt	Bmt	Pullam Fm	Bmt	Bmt
Age (Ma):	1900	1900	1900						∼1100	∼1100
Sill type:	Major (cum)	Major (cum)	Major (cum)							
wt %										
SiO_2	45·87	46·61	49·54	49·95	55·36	51·91	70·01	69·12	36·70	38·37
TiO_2	0·37	0·41	0·54	1·10	0·58	0·51	0·26	0·37	5·33	4·84
Al_2O_3	7·57	8·21	11·50	15·97	14·36	11·11	15·70	14·77	4·18	3·60
Fe_2O_3	13·39	13·43	11·96	13·18	10·59	11·47	2·44	3·61	14·93	14·16
FeO*	12·05	12·08	10·76	11·86	9·53	10·32	2·20	3·25	13·43	12·74
MnO	0·19	0·19	0·18	0·19	0·16	0·18	0·05	0·06	0·21	0·20
MgO	25·15	24·06	15·69	6·35	8·13	13·29	0·94	1·64	22·43	22·99
CaO	5·63	6·20	8·91	10·49	7·86	9·01	2·62	2·53	12·08	11·85
Na_2O	0·62	0·81	1·22	2·29	1·55	1·44	4·50	3·73	0·40	0·35
K_2O	0·31	0·37	0·35	0·52	1·44	0·93	3·06	3·51	2·04	1·67
P_2O_5	0·04	0·05	0·06	0·10	0·10	0·06	0·10	0·14	1·00	1·05
Total	99·13	100·34	99·95	100·14	100·14	99·91	99·68	99·47	99·30	99·08
LOI	2·20	2·10	2·10	1·21	2·00	1·60	1·01	0·91	6·83	6·94
Mg no.	84·20	83·56	78·82	57·75	68·54	76·68	52·22	56·31	81·00	82·16
ppm										
Ba	97	106	93	117	186	157	930	774	1550	1207
Co	106·3	108·2	72·4	44·2	44·8	57·4	7·8	10·6	93·1	89·2
Cr	2857	2898	1452	157	487	1527	18	42	806	691
Cu	48·9	59·5	80·7	168	61·8	66·3	10·7	13·6	130·0	135·8
Ga	n.d.	10·8	13·5	15·9	15·3	12·5	19·6	17·9	9·8	11·8
Hf	1·14	1·51	1·56	1·68	2·48	1·78	1·80	3·37	10·19	11·85
Nb	1·77	2·37	2·55	3·13	5·42	2·42	4·87	7·80	166·00	158·67
Ni	919	919	513	101	153	413	8	18	833	802
Pb	2·33	2·70	3·73	2·86	8·57	5·12	18·47	33·17	9·28	9·77
Rb	14·3	19·2	17·6	22·4	77·2	42·4	82·1	137·7	165·3	133·6
Sc	22·8	28·3	32·7	36·0	30·0	32·1	3·8	7·0	17·7	29·9
Sr	66·4	67·9	84·0	184	121·5	136·5	686	363	1167	927
Ta	0·44	0·77	0·51	0·58	0·73	0·52	0·61	0·75	9·70	11·00

Table 3: continued

Sample:	98MA98	99MA55	99MA56	99MA50	98MA114	99MA60	98MA03	99MA63	98MA119bo	98MA123
Rock type:	Picrite sill	Picrite sill	Dol sill	Dol dyke	Dol dyke	Dol dyke	Granite	Granite	Kimberlite	Kimberlite
Location:	R/S Pul-DC	Pul-DC	Pul-DC	Anj	Kon	Mir	Kur	Ipuru	Mul	Mul
Unit:	Tad Fm	Tad Fm	Tad Fm	Bmt	Bmt	Bmt	Bmt	Pullam Fm	Bmt	Bmt
Age (Ma):	1900	1900	1900						~1100	~1100
Sill type:	Major (cum)	Major (cum)	Major (cum)							
Th	2·57	3·06	3·47	0·96	6·85	2·72	7·89	27·23	16·80	16·57
U	0·51	0·63	0·68	0·23	2·66	0·66	1·24	7·88	3·09	2·79
V	137	117	154	258	213	179	36	61	316	297
Y	8·47	10·63	13·20	18·17	15·47	12·17	7·62	11·80	21·63	20·63
Zn	56·5	74·7	66·2	103·9	86·0	70·7	41·9	47·8	83·6	71·8
Zr	32·8	44·0	48·3	55·5	82·5	56·7	64·2	116·7	410·7	440·0
La	6·40	7·93	9·18	6·37	15·93	9·98	30·83	35·70	130·67	118·00
Ce	15·40	19·10	19·80	17·13	33·27	21·83	58·03	64·97	252·33	231·33
Pr	1·40	1·80	2·06	1·93	3·61	2·36	6·18	6·98	28·93	25·90
Nd	5·83	6·91	8·38	8·53	13·30	9·17	21·03	24·47	102·33	92·13
Sm	1·30	1·53	1·92	2·33	2·86	1·90	3·37	4·02	14·65	13·77
Eu	0·42	0·53	0·64	1·07	0·80	0·66	1·11	1·15	4·47	4·17
Gd	1·64	2·07	2·50	3·15	3·31	2·48	3·47	4·30	14·80	13·33
Tb	0·27	0·32	0·39	0·53	0·50	0·39	0·35	0·48	1·44	1·30
Dy	1·75	2·08	2·52	3·27	2·84	2·24	1·58	2·33	6·17	5·31
Ho	0·36	0·44	0·53	0·77	0·63	0·50	0·29	0·44	0·96	0·89
Er	1·06	1·37	1·63	2·17	1·88	1·56	0·83	1·43	2·17	2·11
Tm	0·17	0·18	0·24	0·30	0·28	0·20	0·12	0·18	0·22	0·24
Yb	1·11	1·22	1·59	2·06	1·78	1·30	0·84	1·04	1·47	1·26
Lu	0·16	0·17	0·24	0·33	0·26	0·18	0·10	0·15	0·16	0·19

Sample:	99MA64	99MA65B	BCR-2	BCR-2	AGV-1		GSP-1		PCC-1	PCC-1
Rock type:	Syenite	Syenite	Basalt		Andesite		Granodiorite	Perid	Perid	
Location:	Racherla	Giddalur								
Unit:	Pullam Fm	Pullam Fm								
Age:										
			This study	USGS	This study	USGS	This study	USGS	This study	This study
wt %										
SiO_2	49·06	47·67	—	54·10	—	58·84	—	—	—	—
TiO_2	3·53	8·27	—	2·26	—	1·05	—	0·65	0·01	0·01
Al_2O_3	5·62	7·25	—	13·50	—	17·15	—	—	—	—
Fe_2O_3	16·25	16·98	—	—	—	—	—	—	—	—
FeO*	14·62	15·28	—	12·42	—	6·09	—	—	—	—
MnO	0·17	0·33	—	—	—	—	—	—	—	—
MgO	4·37	3·78	—	3·59	—	1·53	—	—	—	—
CaO	7·09	5·01	—	7·12	—	4·94	—	—	—	—
Na_2O	4·45	2·74	—	3·16	—	4·26	—	—	—	—
K_2O	5·02	6·74	—	1·79	—	2·92	—	5·51	0·01	0·01
P_2O_5	1·88	0·81	—	0·35	—	0·50	—	0·28	—	—
Total	97·43	99·58	—	98·3	—	97·3	—	—	—	—

Sample:	99MA64	99MA65B	BCR-2	BCR-2	AGV-1		GSP-1		PCC-1	PCC-1
Rock type:	Syenite	Syenite	Basalt		Andesite		Granodiorite	Perid	Perid	
Location:	Racherla	Giddalur								
Unit:	Pullam Fm	Pullam Fm								
Age:										
			This study	USGS	This study	USGS	This study	USGS	This study	This study
LOI	4·20	3·08	—	—	—	—	—	—	—	—
Mg no.	43·28	38·71	—	42·47	—	30·93	—	—	—	—
ppm										
Ba	8321	1370	681	683	1105	1230	1180	1310	2	2
Co	34·7	38·8	—	37	—	15	—	—	—	—
Cr	23	8	—	18	—	10	—	—	—	—
Cu	40·0	5·5	—	19·0	—	60·0	—	—	—	—
Ga	20·2	28·7	—	23·0	—	20·0	—	—	—	—
Hf	27·38	25·83	4·93	4·80	4·96	5·10	2·17	—	0·31	1·00
Nb	188·00	239·00	11·70	—	12·77	15·00	24·97	27·90	0·31	0·50
Ni	6	17	—	—	—	—	—	—	—	—
Pb	26·33	39·50	9·49	11·00	34·17	36·00	48·77	55·00	8·58	8·58
Rb	39·1	65·7	—	48·0	—	67·0	—	254·0	—	—
Sc	19·2	24·8	33·5	33·0	12·0	12·0	6·0	6·2	9·8	9·5
Sr	3725	3828	—	346	—	660	—	—	0·4	0·4
Ta	17·10	16·20	0·89	—	0·99	0·90	0·96	0·97	0·20	0·30
Th	85·80	5·15	6·05	6·20	6·13	6·50	96·47	106·00	0·35	1·28
U	4·41	0·88	1·61	1·69	1·72	1·92	1·95	2·54	0·02	0·04
V	313	226	—	416	—	120	—	—	—	—
Y	40·10	24·60	31·00	37·00	16·77	20·00	21·07	26·00	0·07	0·12
Zn	201·1	317·3	—	127·0		88·0	—	—	—	—
Zr	1126·7	886·7	175·7	188·0	205·7	227·0	70·7	—	0·4	1·0
La	432·33	138·00	24·20	25·00	35·93	38·00	161·67	184·00	0·08	0·09
Ce	830·00	260·67	52·50	53·00	65·37	67·00	384·67	399·00	0·20	0·20
Pr	90·50	29·00	6·56	6·80	7·96	7·60	49·33	52·00	0·02	0·04
Nd	296·67	102·00	27·43	28·00	29·70	33·00	178·00	196·00	0·01	0·03
Sm	33·30	14·90	6·07	6·70	5·32	5·90	22·70	26·30	0·01	0·05
Eu	10·74	4·46	2·09	2·00	1·80	1·60	2·33	2·33	0·01	0·02
Gd	34·83	13·63	7·34	6·80	5·73	5·00	17·03	12·10	0·04	0·09
Tb	2·52	1·50	1·06	1·07	0·67	0·70	1·51	1·34	0·01	0·03
Dy	9·59	6·21	6·15	—	3·43	3·60	5·07	5·50	0·04	0·05
Ho	1·65	1·03	1·26	1·33	0·67	—	0·83	1·01	0·01	0·07
Er	4·33	2·61	3·70	—	1·80	1·70	2·46	2·70	0·03	0·05
Tm	0·42	0·30	0·53	0·54	0·25	—	0·23	0·38	0·01	0·04
Yb	2·19	1·70	3·46	3·50	1·70	1·72	1·36	1·70	0·03	0·09
Lu	0·27	0·25	0·51	0·51	0·23	0·27	0·16	0·21	0·01	0·05

XRF analyses were undertaken at the University of Durham and ICP-MS analyses were carried out at the NERC facility, Kingston University. Details of operating conditions have been described by Anand (2001). Total Fe reported as Fe_2O_3. FeO^* are recalculated values using the formula $FeO^* = XRF\ Fe_2O_3/1{\cdot}11135$; Mg number = [(atomic Mg)/(atomic Mg + atomic Fe)]. Locality abbreviations for sample locations: Anj, Anjanayapuram; Beth, Bethamcherla; bo, bomb; Brah, Brahmanpalli; Pul-DC, Pulivendla Degree College; Gat, Gattimanikonda; Kal, Kalimanigutta; Kon, Konampeta; Kond, Kondapuram; Krish, Krishnagiri; Kur, Kurnool; Mir, Miriyalguda; Mudd, Muddanuru; Mul, Muligiripalli; Pul, Pulivendla; Pullam, Pullampet; Ranga, Rangapuram; Tad, Tadpatri; Vem, Vempalle; Yer, Yeraguntla. Bas, basalt; Bmt, basement; Dol, dolerite; Perid, peridotite; cum, cumulate sill; dif, differentiated sill.

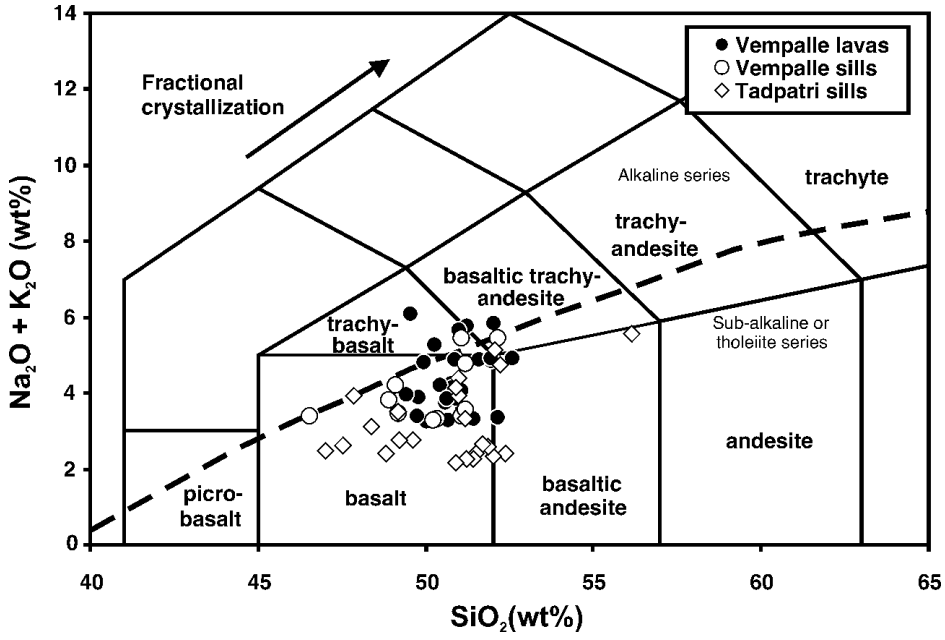

Fig. 4. Bulk-rock analyses of the Cuddapah lavas and sills plotted on the total alkalis vs silica (TAS) diagram of Le Maitre (2002). Only samples considered to be representative of the liquid composition and with LOI value of <3 wt % are plotted. The dashed curve shows the subdivision of alkaline and tholeiitic series of rocks on a TAS diagram, after Irvine & Baragar (1971). The vector illustrates the effects of fractional crystallization.

olivine apex of the Di–Ol–Hy triangle. This suggests that the Tadpatri mafic sills were derived from a parental melt that underwent fractionation at the base of the crust (9·0 kbar) and subsequently experienced olivine accumulation prior to or during the emplacement of the sill complex. This postulated magmatic underplating is consistent with geophysical studies that have indicated the presence of a high-density lopolithic magmatic body below the Papaghni sub-basin (Mishra & Tiwari, 1995).

The 'minor' dolerite and basaltic sills exhibit a narrow range in MgO contents (4–8 wt %). The bulk-rock compositions of these samples seem to have been controlled by clinopyroxene and feldspar fractionation (Fig. 5). This is in agreement with petrographic observations.

Trace-element variation

Both compatible and incompatible trace elements show a relatively restricted range in their abundances in the Vempalle Fm lavas and sills (Fig. 7). Concentration of Cr varies from 22 to 265 ppm and Ni from 25 to 120 ppm. The relatively low Cr and Ni contents are consistent with the absence of olivine and spinel in the Vempalle Fm lavas and sills. Because many of the samples have suffered hydrothermal alteration, concentrations of highly mobile large ion lithophile elements (LILE; e.g. Rb) are variable (Fig. 7). Moderately incompatible elements (e.g. La, Y and Zr) show an overall increase in their concentration with decreasing MgO content (Fig. 7). The Vempalle Fm samples exhibit at least two distinctive trace-element patterns on normalized multi-element plots. The Bethamcherla lavas and a sill sample from Pulivendla show a slight enrichment in moderately incompatible elements (Nd to Lu) compared with other Vempalle Fm samples (Fig. 8a). They also show the strongest depletions in Pb and Sr and have relatively small Nb and Ta anomalies in Fig. 8a. As plagioclase feldspar has a relatively high partition coefficient for Sr and Pb (Rollinson, 1993), the relative depletion of these elements probably indicates the fractionation of this phase from the parental melt. This is also consistent with the dominance of alkali feldspar (albite) over plagioclase feldspar in these samples. The remainder of the Vempalle Fm samples are characterized by (1) slightly lower concentrations of moderately incompatible elements (Nd to Lu) and (2) less marked Sr and Pb depletions compared with the Bethamcherla lava (Fig. 8a), reflecting the presence of both plagioclase and alkali feldspar (albite) in these samples. They show relatively large Nb and Ta anomalies with La/Nb = 2–3.

The Tadpatri sills show a wide range in their trace-element abundances compared with the Vempalle Fm lavas and sills. In the 'cumulate' samples, Cr contents vary from ~1300 to 3000 ppm whereas Ni contents range from 500 to 1000 ppm (Fig. 7). It is clear from Fig. 7 that olivine and spinel control the variation of Cr

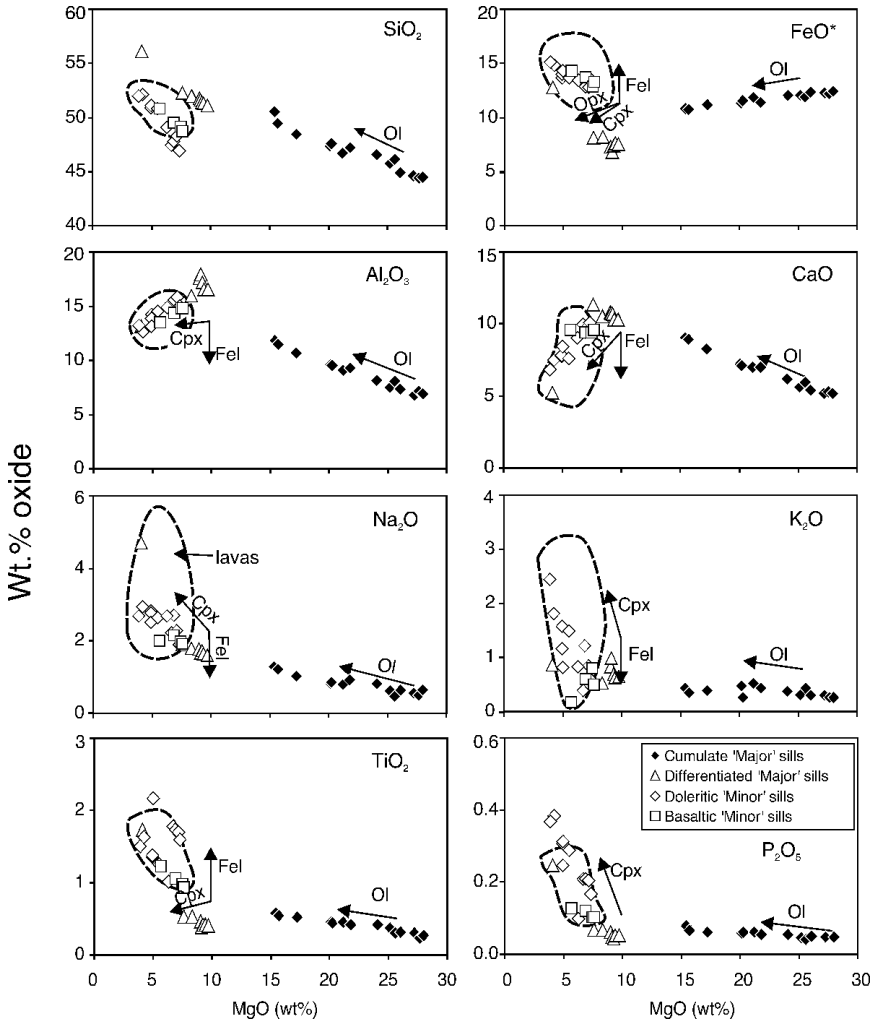

Fig. 5. Harker diagrams showing the variation in concentrations (in wt %) of selected major-element oxides with MgO for the Vempalle Fm lavas and sills and Tadpatri sills. Dashed line encloses the Vempalle Fm dataset. Vectors illustrate the effect of crystal fractionation.

whereas Ni contents are solely controlled by olivine. Similarly, the 'differentiated' sill samples show evidence of olivine and spinel control but there was probably another phase involved in the fractionating sequence. This additional phase could have been orthopyroxene, which is usually present in cumulate portions of the sill. The fractionation trends for Cr and Ni in the 'minor' sills are probably due to olivine crystallization alone (Fig. 7).

Incompatible trace elements (such as Rb and Sr) show an overall increase in their concentration with decreasing MgO in all of the Tadpatri sills; the trend is much clearer in the 'cumulate' sills compared with the 'differentiated' and 'minor' sills (Fig. 7). Because of the cumulate origin of the most MgO-rich Tadpatri sills, the concentrations of incompatible elements are extremely low (e.g. La 3·3 ppm, Nd 3 ppm). Because many of the low-MgO sills are hydrothermally altered, concentrations of some of the highly mobile elements (such as Rb, Sr and Th) may have been affected. La, Y and Zr are less mobile and follow a well-defined fractionation trend in all of the Tadpatri sill samples (Fig. 7).

The Tadpatri sills exhibit similar normalized multi-element patterns to the Vempalle Fm lavas, but the former show smaller variations in abundances of LILE (Fig. 8b). Concentrations of relatively immobile trace elements vary from six to 20 times chondrite. The 'cumulate' rocks have relatively low abundances of moderately incompatible trace elements (Nd to Lu), which are consistent with their high modal olivine contents. Samples from the 'differentiated' and 'minor' sills have slightly elevated concentrations of these trace elements. It is expected that with decreasing MgO content the 'cumulate' samples will show a general enrichment in the abundances of incompatible trace elements. This is not readily apparent from

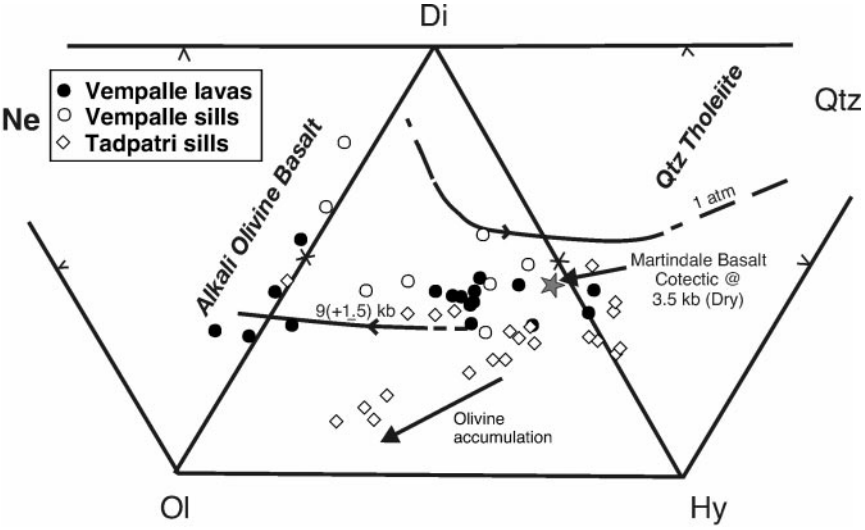

Fig. 6. Comparison of the CIPW normative compositions of the Vempalle Fm lavas and sills and the Tadpatri sills with the results of experimental studies, after Thompson *et al.* (1983). Only samples with >5 wt % MgO and LOI value of <3 wt % are plotted on this diagram.

Fig. 8b but is in agreement with the observation made earlier that the incompatible trace elements such as La, Zr and Y show a scattered correlation with whole-rock MgO content in the 'cumulate' samples (Fig. 7). In contrast to the high field strength elements, the LILE are relatively enriched in the 'cumulate' rocks. Only these rocks and some 'minor' sills show Sr depletions, similar to the Vempalle Fm lavas. The Sr depletions are consistent with the presence of relatively small modal amounts of plagioclase feldspar in the 'cumulate' samples and the dominance of Na-rich feldspars in the 'minor' sills.

Rare earth element variation

Vempalle Fm lavas and sills

The chondrite-normalized REE abundances of representative samples of the Vempalle Fm lavas and sills are shown in Fig. 9. The sills show similar trace-element patterns to some of the lavas. In general, the Vempalle Fm samples are slightly enriched in light REE (LREE) relative to the middle REE (MREE) and heavy REE (HREE) (Fig. 9a); $(La/Sm)_n$ ratios vary from 1·4 to 2·5 and $(La/Yb)_n$ from 2·4 to 4·3. The relatively flat REE patterns of the Vempalle Fm lavas and sills are consistent with their tholeiitic nature. Absolute abundances of the REE vary between nine and 60 times chondrite, with the majority of the samples only enriched up to 40 times chondrite. One of the lavas from Bethamcherla (98MA07) and a sill from Pulivendla (98MA103) exhibit slight Eu depletions (Fig. 9a). This is consistent with plagioclase feldspar fractionation, previously identified by relative depletions in Sr. Also, the Bethamcherla lava is depleted in LREE relative to other Vempalle Fm lavas, which may be due to clinopyroxene fractionation. Sample 99MA37 from Animala shows a positive Eu anomaly, which is in agreement with the relatively high modal proportion of plagioclase feldspar in this sample.

Tadpatri sills

The abundances of HREE in the Tadpatri sills vary from five to 25 times chondrite whereas LREE abundances vary from 20 to 80 times chondrite (Fig. 9b). Similar to the Vempalle Fm lavas, the Tadpatri sills show relative enrichments in their LREE concentrations compared with MREE and HREE; $(La/Sm)_n$ ratios vary from 1·2 to 3·2 and $(La/Yb)_n$ from 2·3 to 5·3. Samples from the 'cumulate' portions of the sills are highly depleted in MREE and HREE (Fig. 9b) but they show enrichment in LREE and have relatively high $(La/Sm)_n$ ratios (1–3). With decreasing whole-rock MgO content, i.e. decrease in modal olivine content, the concentration of REE increases. Some of the samples from the granophyric portions of the sill complex show moderate enrichment in the LREE (Fig. 9b).

The 'minor' sills show limited enrichments in their LREE contents; they have relatively low $(La/Sm)_n$ and $(La/Yb)_n$ ratios in the range of 1·2–2 and 2·3–3·5, respectively. This indicates that these sills may have had a different petrogenesis compared with the sills from the Tadpatri mafic–ultramafic sill complex.

Variations in Sr- and Nd-isotopic ratios

Sr and Nd isotope determinations were carried out on a representative suite of mafic sills and lavas from the

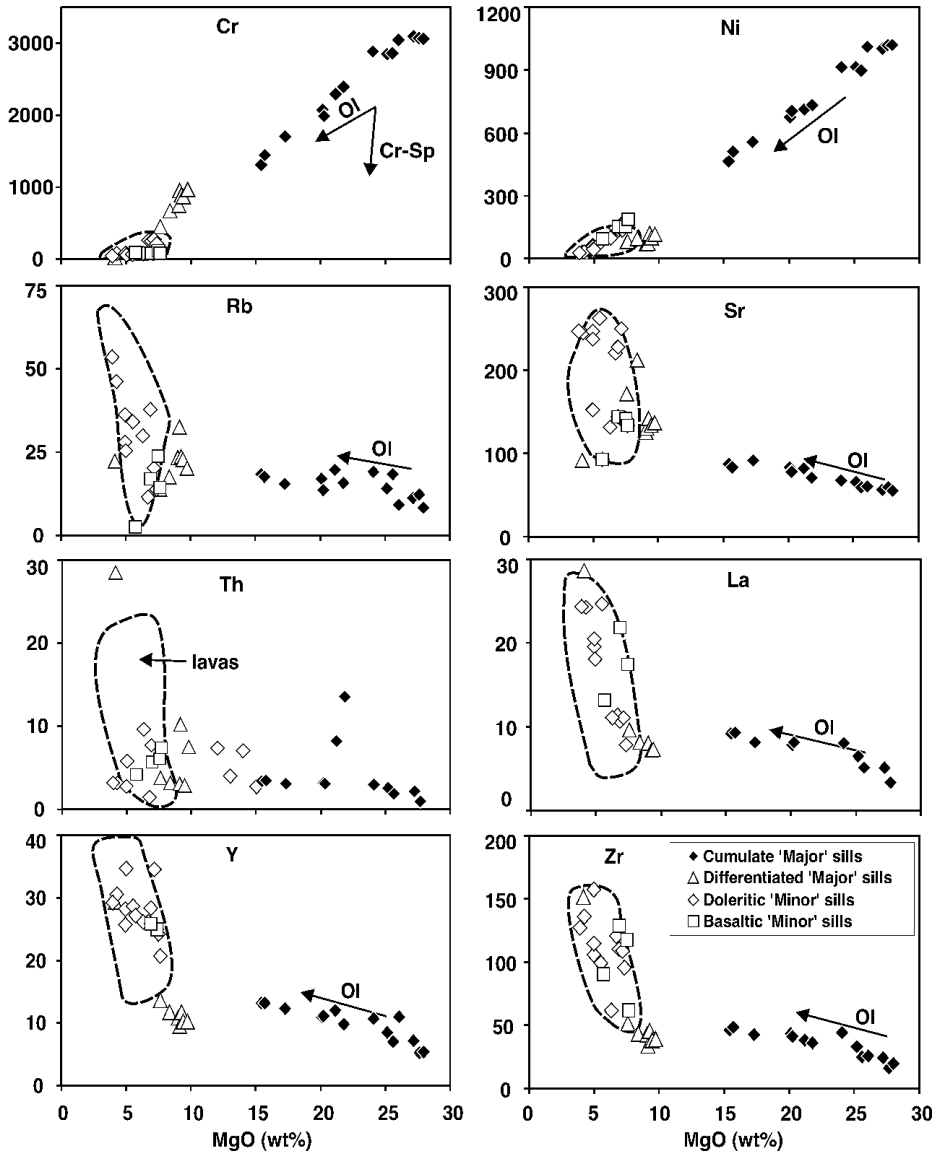

Fig. 7. Variation of selected trace-element concentrations (in ppm) with MgO (in wt %) of the Vempalle Fm lavas and sills and Tadpatri sills. Dashed line encloses data for Vempalle Fm samples. Vectors illustrate the effect of crystal fractionation.

Cuddapah Basin (Table 4). The selected samples are petrographically fresh and have LOI $<2{\cdot}5$ wt %. Initial ratios were calculated to 1900 Ma. The samples exhibit a moderate range in $^{87}Sr/^{86}Sr_i$ ratios (0·70562–0·7081) and ε_{Sr} values range from 5·5 to 8·5. We are cautious about the significance of these Sr-isotopic ratios, given the susceptibility of Rb to mobilization in rocks of this age. Nevertheless, we note that the samples exhibit a positive co-variation with Nd isotopes in Fig. 10. This suggests that either the $^{87}Sr/^{86}Sr_i$ ratios have been affected by the same degree of post-magma genesis alteration or that the effects of this process are limited. The Cuddapah samples exhibit a wide range of $^{143}Nd/^{144}Nd_i$ ratios (0·51023–0·50967) that are similar to or lower than that of bulk-Earth at 1900 Ma (0·51018); these correspond to ε_{Nd} values of one to -10. The low negative ε_{Nd} values suggest that the parental magmas of most of the sills and lavas contain melt contributions from Archaean lithosphere. The Cuddapah samples do not appear to exhibit a systematic variation between radiogenic isotopic ratios and MgO content. Furthermore, there is no obvious difference between the Sr and Nd isotopic signatures of the sills and lavas. The sample with the highest ε_{Nd} value, i.e. the least contaminated, is a lava flow from Animala (99MA34).

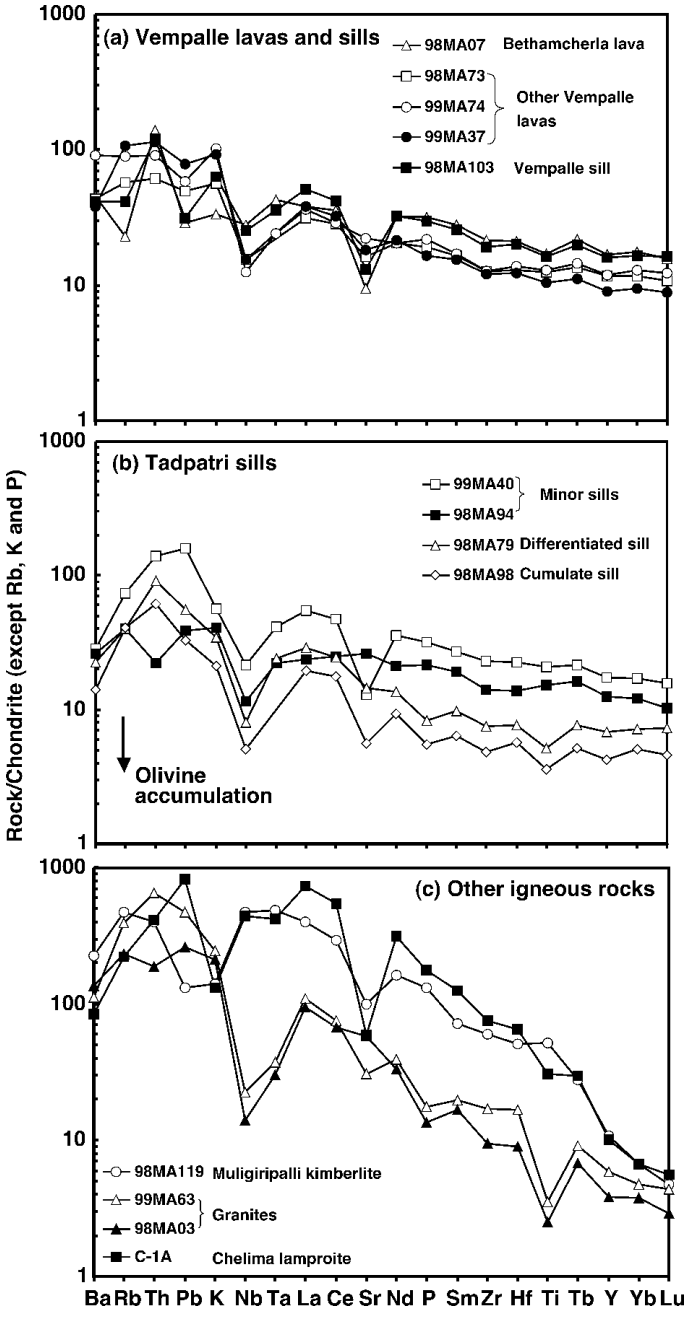

Fig. 8. Normalized plot of incompatible trace-element abundances in representative samples from: (a) Vempalle Fm lavas and sills; (b) Tadpatri sills; (c) additional igneous rocks from in and around the Cuddapah Basin. Normalization factors are chondritic, except for Rb, K and P, which are normalized to bulk-Earth values (Thompson *et al.*, 1984). The vector shows the effect of olivine accumulation on the trace-element patterns in (b).

PETROGENESIS

The petrographic, mineralogical and geochemical characteristics of the mafic lavas and sills from the Cuddapah Basin have highlighted the involvement of complex magma chamber processes in their petrogenesis. To understand the nature of the melt generation processes and the role of the convecting mantle, it is necessary to assess the role of lithospheric contamination.

Lithospheric contamination

We have used trace-element and isotopic ratios to assess the relative roles of melts derived from the lithospheric

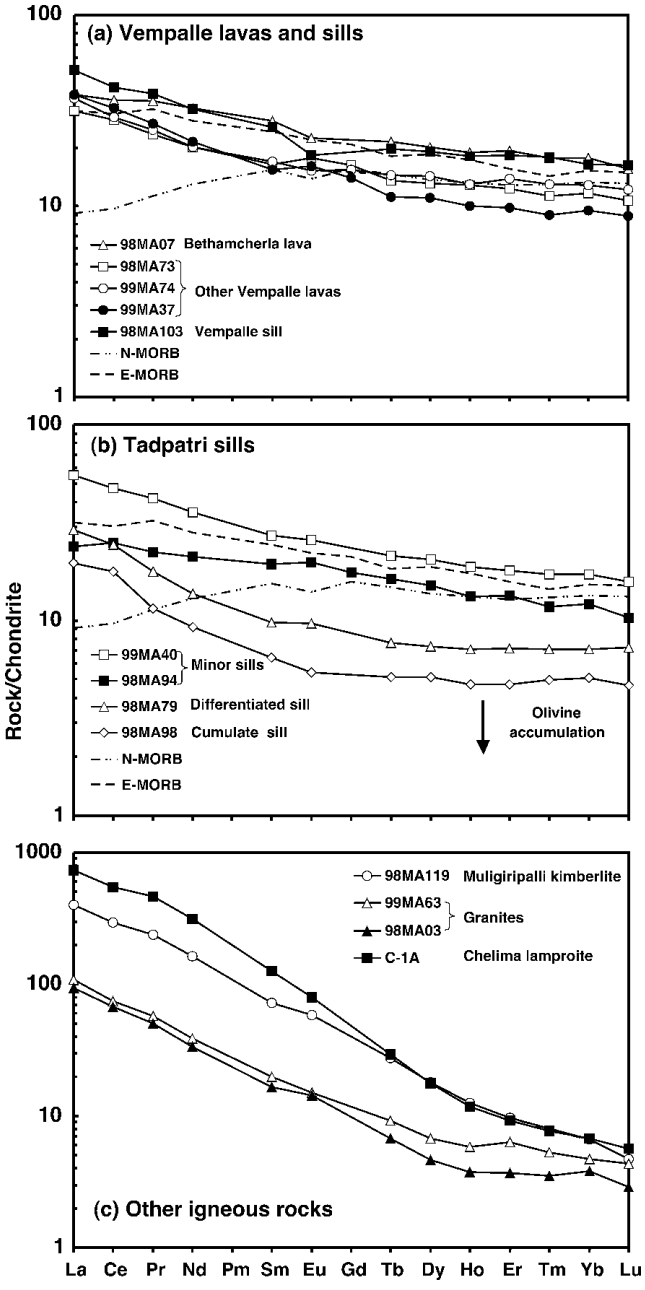

Fig. 9. Chondrite-normalized plot of REE abundances in representative samples from: (a) Vempalle Fm lavas and sills; (b) Tadpatri sills; (c) additional igneous rocks from in and around the Cuddapah Basin. Normalization factors are from Nakamura (1974), except for Pr, Tb, Ho and Tm, which are from Wakita *et al.* (1971). Vector illustrates the effect of olivine accumulation on REE concentrations. N-MORB and E-MORB are also plotted in (a) and (b) for comparison. The MORB data are from PETDB (Petrological database of the ocean floor), available at http://petdb.ldeo.columbia.edu/petdb/enterdatabase.htm.

mantle and/or continental crust. We have assumed that the compositions of the Proterozoic kimberlites and lamproites from in and around the Cuddapah Basin are representative of melts derived from metasomatized continental lithospheric mantle (e.g. McKenzie, 1989; Gibson *et al.*, 1995). These are characterized by extreme enrichments in LREE and HFSE [$(La/Yb)_n = 50–125$, $La/Nb = 0{\cdot}7–1{\cdot}5$)] and relative depletions at Sr on normalized multi-element plots (Chalapathi Rao *et al.* (1998); Figs 8c and 9c). The kimberlites and lamproites are characterized by different Sr and Nd isotopic ratios. Model age calculations, relative to depleted mantle, indicate that their parental melts contain contributions from lithospheric mantle that was

Table 4: Sr and Nd isotopic ratios of samples of Proterozoic mafic igneous rocks from the Cuddapah Basin

	Lithology	$^{40}Ar/^{39}Ar$ (Ma)	$^{87}Sr/^{86}Sr_m$	$^{87}Sr/^{86}Sr_i$	ε_{Sr}	$^{143}Nd/^{144}Nd_m$	$^{143}Nd/^{144}Nd_i$	ε_{Nd}
98MA7	Basalt	1900	0·71380	0·70815	8·37	0·512169	0·510066	−2·23
99MA34	Basalt	1900	—	—	—	0·512183	0·510234	1·06
98MA24	Basalt	1900	0·72191	0·70726	7·11	0·511660	0·509814	−7·17
98MA73	Basalt	1900	0·71400	0·70562	4·78	0·512156	0·510167	−0·26
98MA76	Basalt	1900	0·71994	0·70675	6·38	0·511966	0·510130	−0·97
98MA97	Basalt	1900	0·72260	0·70625	5·67	0·511704	0·509904	−5·40
98MA98	Basalt	1900	0·72454	0·70751	7·46	0·511673	0·509979	−3·93
99MA74	Basalt	1900	—	—	—	0·511731	0·509677	−9·86
C5	Lamproite	1417	0·72229	0·71689	19·98	0·511157	0·510461	−6·78
ZP	Lamproite	1417	0·74115	0·72210	27·40	0·511219	0·510441	−7·17
NR/1	Lamproite	1417	0·74462	0·73907	51·54	0·511335	0·510501	−6·00

$^{40}Ar/^{39}Ar$ ages are from this work and Chalapathi Rao *et al*. (1999). Measured isotopic ratios of Cuddapah lamproites are from Chalapathi Rao *et al*. (1998). Concentrations of Rb, Sr, Nd and Sm, used to calculate initial isotopic ratios, are from Table 3 and Chalapathi Rao *et al*. (1998). Sr and Nd isotope determinations were undertaken at McMaster University. Details of analytical techniques have been given by Gibson *et al*. (1999).

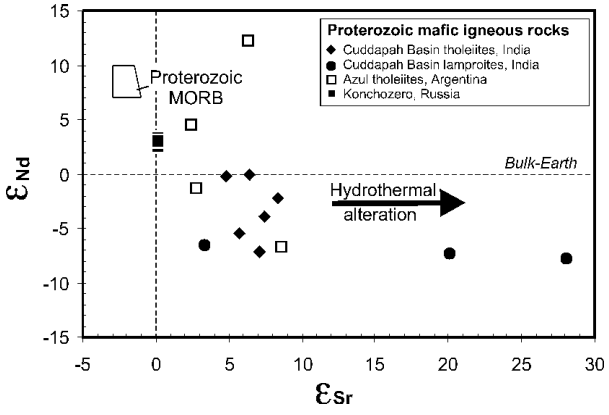

Fig. 10. Variation of Sr and Nd isotopes in mafic igneous rocks from the Cuddapah Basin. Epsilon Sr and Nd values are also shown for other worldwide occurrences of Proterozoic mafic igneous rocks. Data sources: Table 4; Chalapathi Rao *et al*. (1998); Puchtel *et al*. (1999); Iacumin *et al*. (2001).

metasomatized between 3000 and 1900 Ma (Chalapathi Rao *et al*., in preparation). This suggests that readily fusible metasomatized lithospheric mantle may well have been present beneath the Cuddapah Basin at the time of genesis of the sills and lavas that are present in the Vempalle and Tadpatri Formations. Nevertheless, both the kimberlites and lamproites are characterized by low La/Nb ratios relative to the contaminated lavas and sills (Fig. 8c). This suggests that the latter contain melt contributions from a different lithospheric source, perhaps from the local continental crust.

Basement granite samples in the vicinity of the Cuddapah Basin have been assumed to provide an estimate of the crustal end-member. The granites show an enrichment in LILE but are characterized by very pronounced negative Nb, Ta and Ti anomalies (Fig. 8c). These samples have $(La/Yb)_n$ ratios (25–30) that are lower than the mafic–potassic samples but are significantly higher than those of the Cuddapah lavas and sills [$(La/Yb)_n$ = 3–4]. The normalized Nb, Ta and, to a certain extent, Ti contents of the Cuddapah lavas and sills show variations similar to those of the granite samples in Fig. 8. This observation indicates the possible role of crustal contamination. The lack of correlation between indices of fractionation (e.g. MgO) and Nd-isotopic ratios suggests that the assimilation was more complex than can be attributed to assimilation and/or fractionation in a single magma chamber.

Figure 11a shows a plot of Sm/Yb vs La/Sm for the Cuddapah lavas and sills. The calculated isobaric accumulated fractional-melting curves for both garnet peridotite and spinel peridotite are also plotted together with representative analyses of normal mid-ocean ridge basalt (N-MORB), ocean island basalt (OIB) and 'local' continental crust. It is clear from Fig. 11a that the Cuddapah samples have similar Sm/Yb ratios to N-MORB but they have higher La/Sm ratios. This figure is meant to highlight two major points: (1) the Cuddapah lavas and sills plot along the isobaric accumulated fractional-melting curve for spinel lherzolite, suggesting that they have been derived by mantle melting in the spinel stability field; (2) the Vempalle lavas and some of the non-cumulate Tadpatri sills form a pattern trending towards the

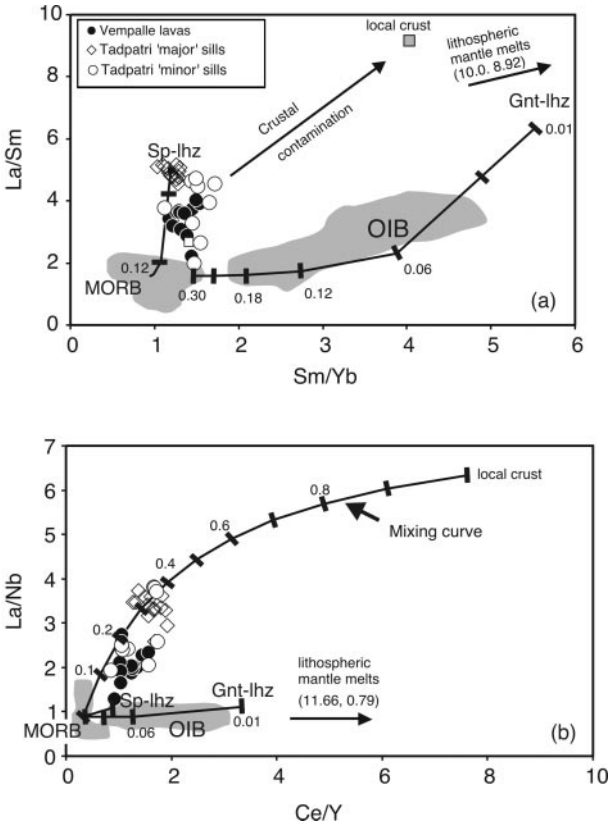

Fig. 11. (a) Plot of Sm/Yb vs La/Sm for the Vempalle Fm lavas and the Tadpatri sills. Vectors illustrate the effect of crustal- and lithospheric-mantle contamination on trace-element ratios. Representative analyses of N-MORB, OIB and the 'local' crust (□) are plotted for comparison. MORB and OIB data are from PETDB (Petrological database of the ocean floor), available at http://petdb.ldeo.columbia.edu/petdb/enterdatabase.htm, and the 'local' crust data are from this work. (b) Plot of Ce/Y vs La/Nb for the Vempalle Fm lavas and the Tadpatri sills. Mixing curves are calculated for variable mixtures of ~20% partial melt (pm) of spinel lherzolite and crustal end-member.

crustal end-member, suggesting involvement of crustal contamination in their genesis. It is important to notice from Fig. 11a that the majority of the cumulate sills show greater enrichment in their La/Sm ratio than the maximum possible enrichment predicted by the calculations. Caution must be taken in interpreting such observations, as elevated La/Sm ratios in these samples could well be caused by a combination of cumulate processes as well as crustal contamination. Other supporting pieces of evidence (e.g. petrographic data, other trace-element data) should be considered in assigning the dominant role to either of the processes. Another interesting feature is the restricted variation in the Sm/Yb ratio of the Cuddapah lavas and sills compared with the wide variation in their La/Sm ratios. If the magmas are mainly derived from the convecting mantle, and have not been significantly contaminated by lithospheric melts, they should exhibit a positive correlation between these two ratios as seen for the N-MORB data. However, a wide variation in La/Sm ratio with restricted Sm/Yb values seems to indicate contamination by the continental crust; contamination by small-fraction lithospheric mantle melts would shift these trace-element ratios towards high La/Sm and Sm/Yb values relative to the N-MORB data.

Figure 11b shows a plot of Ce/Y vs La/Nb for the Cuddapah lavas and sills. The calculated isobaric accumulated fractional-melting curves for both garnet lherzolite and spinel lherzolite are also shown together with representative analyses of N-MORB, OIB and 'local' continental crust. The initial concentrations and partition coefficients for Nb and Y used in melting calculations are for bulk-silicate Earth (Kostopoulos & James, 1992) and are assumed to be similar to those of primitive mantle. Mixing curves have been constructed for trace-element ratios in variable proportions of crustal and primary mantle melts. It is assumed that melts derived from ~20% partial melting of the spinel lherzolite may approximate the parental melts for the Cuddapah lavas and sills. It is apparent from Fig. 11b that the La/Nb and the Ce/Y ratios in the majority of the Cuddapah lavas and some of the sills may be modelled as a mixture of ~10–15% 'local' continental crust and primary mantle melts. In the case of some 'minor' and many of the 'cumulate' sills, however, a significantly larger proportion (20–35%) of crustal assimilation is predicted by this modelling. Nevertheless, it must be emphasized that the cumulate nature of these sills complicates such straightforward interpretations and thus caution should be taken in interpretation of data. In general, the mafic–ultramafic sills are more contaminated than the lavas, which is consistent with the derivation of the former from relatively high-temperature magmas. Although the elevated La/Nb ratios of the ultramafic sills (Fig. 11b) may partly be due to their cumulate origin, some of the 'minor' dolerite sill samples also show relatively high La/Nb ratios, and larger degrees of crustal contamination may not be completely ruled out.

Forward major- and trace-element modelling

The major-element, trace-element and REE data for samples from the mafic–ultramafic sill complex clearly indicate that their bulk-rock compositions are not representative of their parental melts. A large number (~500) of olivine grains were analysed by electron microprobe. The maximum Fo content observed in each sample has been used to estimate the Mg number of the equilibrium melt (Fig. 12), using a $^{Fe-Mg}_{ol-liq}K_d$ value of 0·32, which is appropriate for 9·0 kbar pressure (Ulmer, 1989). In Fig. 12, the bulk-rock compositions

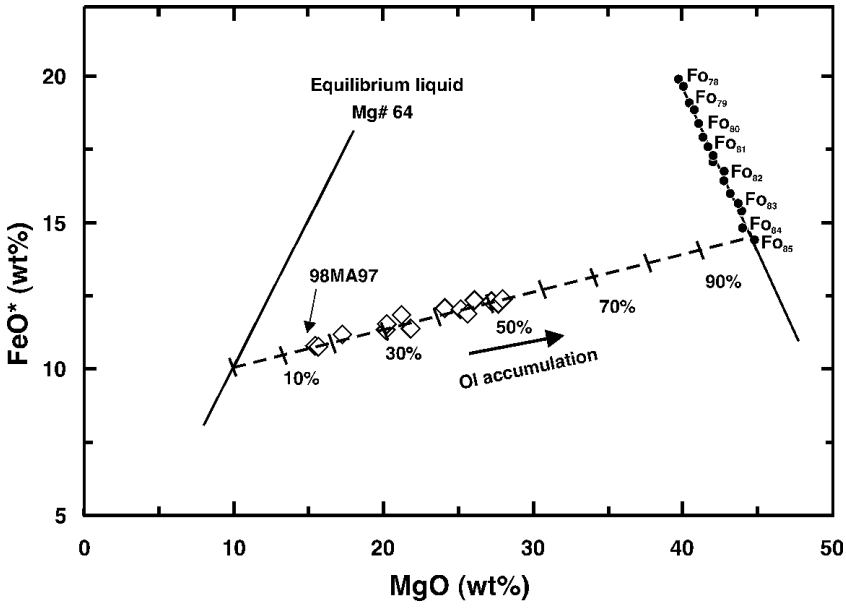

Fig. 12. Tie-lines joining olivine compositions with their equilibrium liquid MgO/FeO* ratios at a given whole-rock MgO content for the Tadpatri mafic–ultramafic sills. The highest Fo content of olivine in each sample is also provided. Tick marks indicate the effects of olivine accumulation.

of the Tadpatri mafic–ultramafic sill complex plot between the equilibrium melt curve and the olivine composition of a given sample. Sample 98MA97 has undergone the least olivine accumulation (~15%), and contains the most Mg-rich olivine (Fo 84·7). The estimated MgO and FeO* contents of the parental liquid for this sample are ~10·0 and 10·1 wt %, respectively.

We have used the approach of Langmuir *et al.* (1992) to investigate the effects of adiabatic decompression melting below the Cuddapah Basin during the Early Proterozoic. Nd and FeO* contents in the Cuddapah lavas and sills have been normalized to 10 wt % MgO (i.e. Nd_{10} and Fe_{10}), by linear regression analysis to correct for low-pressure and/or sub-crustal crystallization. Parameterized K_d values for Nd and Fe in the mantle mineral assemblages have been used to calculate the Nd and Fe contents in the melt at various pressures and degrees of partial melting. Because Nd is strongly partitioned in clinopyroxene, its concentration in the partial melt is predominantly controlled by the clinopyroxene in the parent peridotite. Fe is compatible in almost all of the mantle minerals, with the strongest affinity for olivine. Herzberg & Zhang (1996) determined $K_{d\,Fe}$ in olivine as a function of pressure, which is given by the following equation:

$$K_d(\mathrm{Fe, Ol/L}) = \exp[-0{\cdot}907 + (2{\cdot}415/\mathrm{P})].$$

$K_{d\,Nd}$ values for orthopyroxene and $K_{d\ Fe}$ values for clinopyroxene, orthopyroxene, spinel and garnet are taken from Gibson *et al.* (2000) and McKenzie & O'Nions (1991). Experimental data for the solidus temperature and pressure for fertile peridotite KLB-1 (Herzberg *et al.*, 2000) were used to parameterize Nd and Fe partition coefficients in mantle mineral assemblages. Appropriate non-modal batch and accumulated fractional-melting equations were used to calculate the Nd and Fe content in the partial melts at various stages of adiabatic decompression melting. The modal contents of constituent minerals and their melting proportions are taken from Kostopoulos & James (1992) and are assumed to closely approximate to fertile peridotite KLB-1. The garnet–spinel transition zone is fixed over a pressure range of 25–30 kbar. In all of the calculations, it is assumed that 1·2% melting occurs for every pressure drop of 1 kbar and 1% melt is retained in the source regions as a result of the surface tension of the liquid (Langmuir *et al.*, 1992).

Post magma genesis fractionation and accumulation corrected bulk-rock Nd and FeO* contents of the Cuddapah lavas and sills are plotted in Fig. 13 together with the results of quantitative modelling. The amount of accumulated fractional melting predicted is slightly larger than for the batch-melting model. As polybaric fractional melting is believed to closely approximate to adiabatic decompression melting of the mantle, this is considered to provide more accurate results for the generation of the Cuddapah lavas and sills. The estimated initial pressures of melting vary from ~35 to 40 kbar whereas the top of the melting interval occurs between ~27 and 30 kbar (Fig. 13). The latter is assumed to represent the base of the mechanical

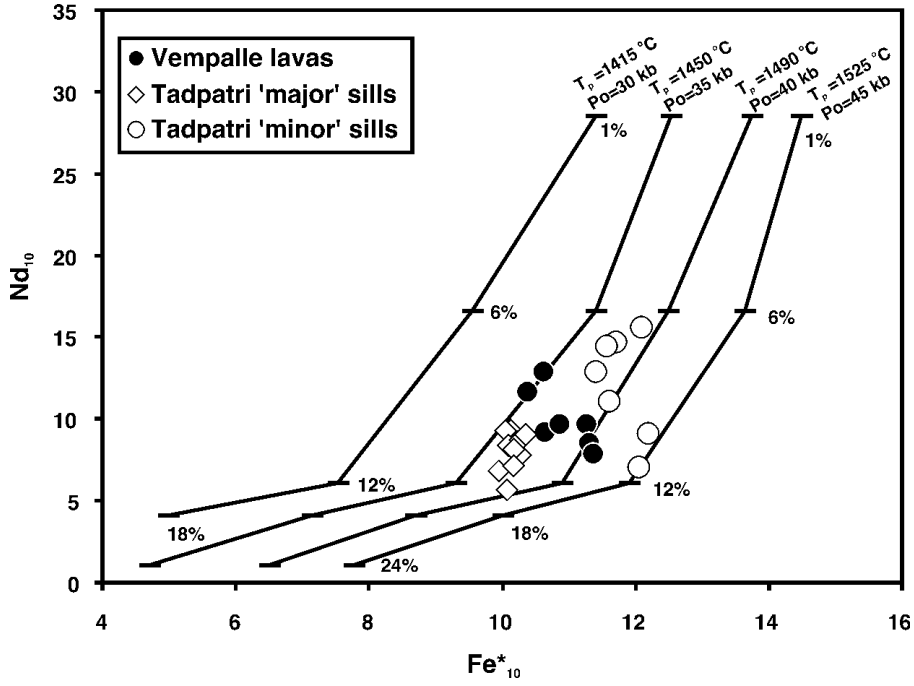

Fig. 13. Variation in Fe^*_{10} and Nd_{10} during polybaric accumulated fractional melting of a fertile peridotite KLB-1 (after Langmuir *et al.*, 1992). These are assumed to represent point and depth average compositions of melts in a 'column' of mantle undergoing adiabatic decompression. Bulk-rock FeO* and Nd contents are normalized to 10 wt % MgO for samples with LOI <3 wt %.

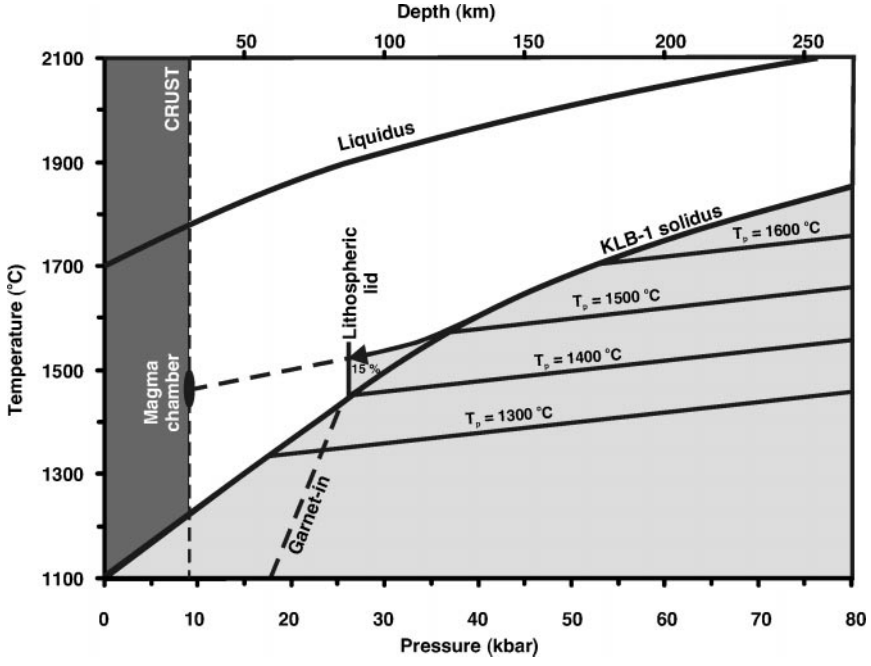

Fig. 14. Results of forward major- and trace-element modelling compared with the results of experimental studies on fertile peridotite KLB-1 (Herzberg *et al.*, 2000). The liquid + solid adiabat is calculated for an entropy of fusion of 250 J/kg (McKenzie & Bickle, 1988). The lithospheric lid corresponds to the base of the sub-Cuddapah Basin mechanical boundary layer, which is estimated to have been at ~80 km depth.

boundary layer (MBL) beneath the Cuddapah Basin. The lavas and 'major' sills appear to have been derived by ~10–15% partial melting, whereas the 'minor' sills were derived from slightly smaller degrees of partial melting (~6–10%). Figure 14 is a pressure vs temperature graph (Herzberg *et al.*, 2000), which illustrates the path of primary peridotite (KLB-1) melts for the Cuddapah sills as a consequence of adiabatic

decompression melting. The estimated mantle potential temperature (T_p) is ~1500°C.

We acknowledge that there are certain limitations with using forward major- and trace-element modelling for the Cuddapah Basin magmas. The most important is the lack of experimental data on Nd and Fe partition coefficients for orthopyroxene, garnet and spinel at relatively moderate pressures (20–35 kbar). In addition, the assumption of the mantle source mineralogy may also have considerable effects on the results. In principle, the starting mantle source mineralogy and its melting proportions should be used for the same peridotite on which most of the experimental data are obtained. Unfortunately, at present not all of this information exists for a single peridotite sample. Assimilation of some crustal material may also affect Nd concentration in mafic samples and we have therefore obtained further petrogenetic information from independent modelling techniques. However, it can qualitatively be seen from Fig. 13 that accounting for crustal contamination will only displace the data towards lower Nd values, i.e. towards slightly higher degrees of partial melting, and thus will not significantly change our results.

REE inversion modelling of the Cuddapah magmas

REE inversion modelling was carried out using the program INVMEL (McKenzie & O'Nions, 1991). This uses the REE concentrations of mafic igneous rocks to calculate the melt-fraction distribution in the mantle during adiabatic decompression melting. In the inversion modelling technique used here, it is assumed that melt extraction is by fractional melting and the observed compositional range is considerably smaller than that of individual primary melts. Some process, therefore, must mix melts from different depths and the average observed melt composition reflects the average compositions of the melts that are generated. Another significant assumption in the modelling is the major-element composition of the source regions.

The results of the REE inversion modelling may be non-unique and it is important to obtain independent constraints for the variables that are required to be specified *a priori*. The most important ones are: (1) depth of the top of the melting column; (2) depth at which initial melting started; (3) mantle source composition; (4) depth of the spinel–garnet transition zone. This transition is fixed between 90 and 100 km based on results of the experimental studies (Klemme & O'Neil, 2000) and the predicted thermal regime of the Earth during the Early Proterozoic (Richter, 1988). The mantle source composition is also fixed for a mixture of primitive and depleted mantle corresponding to an ε_{Nd} value of 4–5 for Early Proterozoic mantle (O'Nions, 1992; McKenzie & O'Nions, 1998).

A number of forward models were obtained by varying values for the top of the melting column and the initial depth of melting. After applying several combinations, those values were chosen that provided the best fit to the observed REE concentrations in samples and yielded a linear melt-fraction distribution curve. Subsequently, these values were used to invert the concentrations of the REE in the Cuddapah lavas and sills to obtain the distribution of the melt fraction through the melting interval, and were also used to predict a fit to the whole-rock trace-element (LILE and HFSE) and major-element data.

REE inversion modelling of the Vempalle Fm lavas

The results of REE inversion obtained for the Cuddapah lavas from Gattimanikonda are illustrated in Fig. 15a. The fractionation-corrected melt distribution curve roughly follows the mantle adiabat for a potential temperature of ~1500°C and provides an estimate of the mantle potential temperature below the Cuddapah Basin during the melt generation event (Fig. 16). The predicted melt-fraction distribution has been used to estimate the trace- and major-element concentrations in the samples.

Trace-element ratios indicate that the Cuddapah Basin lavas have assimilated continental crust; this may explain their elevated LREE and LILE abundances along with relative Nb and Ta depletions. A number of published chemical compositions of the Precambrian upper, middle and lower continental crust (Taylor & McLennan, 1981; Thompson *et al.*, 1982; Weaver & Tarney, 1984; Rollinson, 1993) were used, along with the composition of a granite from inside the Cuddapah Basin (Table 3), to model the degree of crustal contamination in the Cuddapah lavas and sills. The best fit was obtained by using the trace-element data of the 'local' granite sample, which is assumed to approximate the upper continental crustal composition beneath the Cuddapah Basin. It is apparent from Fig. 15b that it is not possible to obtain a best fit for every trace element. Nevertheless, the elevated LREE, U, Th and Pb abundances, and to a certain extent the Nb and Ta depletions, can be modelled reasonably well using 'local' crust as a possible contaminant. The most noticeable discrepancy is the misfit for the Sr and LILE data (e.g. Ba). As mentioned earlier, because the majority of the Cuddapah samples have undergone hydrothermal alteration, it is difficult to interpret the variation in LILE. Such processes may affect concentrations of Sr, but it may also be possible that the fusible crust immediately below the Cuddapah

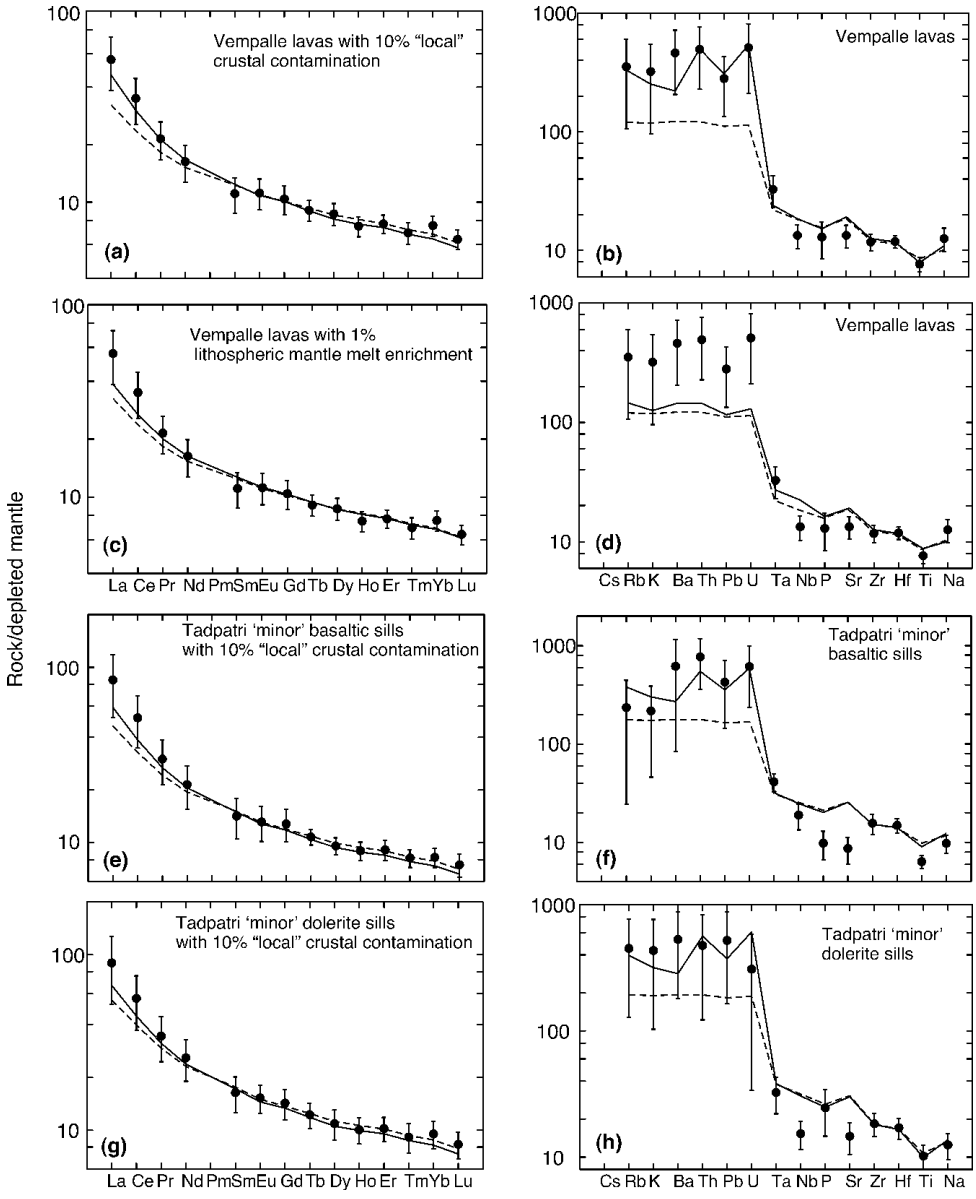

Fig. 15. Results of the REE inversion modelling of the Cuddapah mafic igneous rocks. (a, b) REE concentrations in Vempalle Fm lavas from Gattimanikonda, normalized to MORB source (McKenzie & O'Nions, 1991). •, mean observed concentration ratios; error bars correspond to 1 SD. The plots on the left are those showing best fits (continuous line) for REE and those on the right are the calculated trace-element concentrations for the given best fit (error bars corresponding to 1 SD). The dashed lines show the REE and trace-element fits without crustal contamination. (c, d) Results of REE inversion modelling of Vempalle lavas from Gattimanikonda with 1% enriched lithospheric mantle contamination. (e, f) Results of REE inversion modelling of Tadpatri 'minor' basaltic sills from Krishnagiri and Banganpalle. (g, h) Results of REE inversion modelling of Tadpatri 'minor' dolerite sills. Only samples with $\geq$5 wt % MgO are used for inversion modelling.

Basin is slightly different in its Nb, Ta and Sr concentrations from the granite sample that we have used in the modelling.

We have also considered another scenario in which the parental melts to the Cuddapah lavas were contaminated by lithospheric mantle melts. We have used a 'local' kimberlite sample as our enriched lithospheric mantle end-member. Results of REE inversion for this scenario are shown in Fig. 15c and d. It can clearly be seen that although the enrichment of parental melts by 1% lithospheric melts produces a good fit between the observed and predicted REE data, it fails to produce a good fit to the observed trace-element data. This confirms our previous findings that the parental

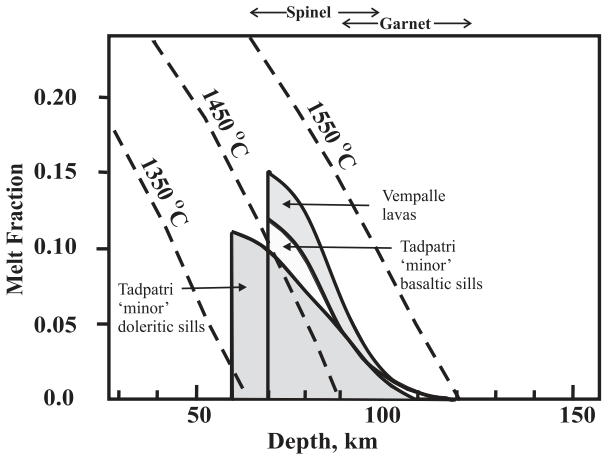

Fig. 16. Melt-fraction distribution curves obtained from inversion modelling of the REE abundances of Cuddapah mafic igneous rocks. Each melt-fraction distribution curve follows a mantle adiabat of ~1500°C, consistent with the results of forward geochemical modelling. All of the Cuddapah mafic igneous rocks seem to have been derived by ~10–15% partial melting of the Early Proterozoic mantle beneath the Cuddapah Basin.

melts to Cuddapah mafic igneous rocks were variably contaminated by continental crust, and have little or no contribution from enriched lithospheric mantle.

REE inversion of the Vempalle Fm lavas from Vempalle, Pulivendla and Animala yields similar results to that of lavas from Gattimanikonda. In general, there is an excellent fit between the observed and predicted REE, trace- and major-element abundances in these lavas. However, the lavas from Animala seem to have assimilated slightly larger degrees of crustal material (15%) than the Gattimanikonda lavas (10%). Nevertheless, in both cases the total amount of melt generated is similar (~15%) and the melt-fraction distribution curve follows the mantle adiabat for a potential temperature of ~1500°C. In contrast, although REE inversion of the Vempalle Fm lavas from Bethamcherla produces an excellent fit between the predicted and the observed REE abundances, the misfit between the predicted and observed trace-element abundances is rather large. In addition, the melt-fraction distribution curve indicates that Bethamcherla lavas were generated by small degrees of partial melting (<6%). The pronounced misfits between observed and calculated Pb, Sr, Na and Ca abundances are consistent with the petrographic evidence; this clearly shows the dominance of sodic feldspar over more calcic feldspar in these samples. Furthermore, these lavas are relatively enriched in incompatible trace elements and REE, and show the least Nb and Ta depletions relative to other Vempalle Fm lavas. Although the REE abundances in the Bethamcherla lavas can be inverted to obtain the melt-fraction distributions, it is important to note that the large misfits between observed and predicted values for many trace- and major-element concentrations probably suggest that they may have a different petrogenetic history from other Vempalle Fm lavas.

REE inversion modelling of the Tadpatri sills

Most samples of the Tadpatri sills exhibit evidence of olivine accumulation and are not suitable for REE inversion. Nevertheless, 'minor' basaltic sill samples, collected from the close vicinity of the 'differentiated' sill complex, near Banganpalle, may be representative of liquid compositions, and thus we have attempted to model the REE abundances in these. A reasonable fit was obtained for the observed and predicted REE concentrations with 10% 'local' crustal contamination (Fig. 15e). However, there are pronounced misfits in the case of P and Ti, and Sr concentrations (Fig. 15f). The P and Ti anomalies may suggest an association of these sills with the cumulate sill complex; both of these elements are abundant in the late-stage granophyres. The melt-fraction distribution predicted for the 'minor' basaltic sills is very similar to that of the lavas (Fig. 16).

The REE concentrations of the 'minor' dolerite sill samples were also inverted (Fig. 15g). Unlike the 'minor' basaltic sills, there is a good fit between the observed and predicted P and Ti concentrations. Other trace elements also show a good fit, except Sr and Nb (Fig. 15h). There is an important point to notice about the 'minor' doleritic sills. They seem to have been derived by smaller degrees of partial melting (10%), with the top of the melt column at a slightly shallower depth (60 km) than the lavas and 'minor' basaltic sill samples (Fig. 16). This observation is consistent with the results of the forward major- and trace-element modelling discussed above.

Discussion of melting models

The results of the REE inversion modelling of the Cuddapah lavas and sills are consistent with the results of the forward major- and trace-element modelling. The melt distribution curves, obtained from the inversion modelling, for the majority of the lava and sill samples, suggest that they have been generated by moderate degrees of partial melting (10–15%) of anhydrous peridotite at a mantle potential temperature of ~1500°C. The estimated initial depth at which mantle melting started varies from 120 to 110 km and the predicted top of the melting column ranges between 60 and 70 km, with most of the melting taking place in the spinel stability field.

REE inversion modelling produces a good fit to the observed REE and trace-element abundances in these samples when variable amounts of 'local' continental crustal contamination (10–15%) are included. In all

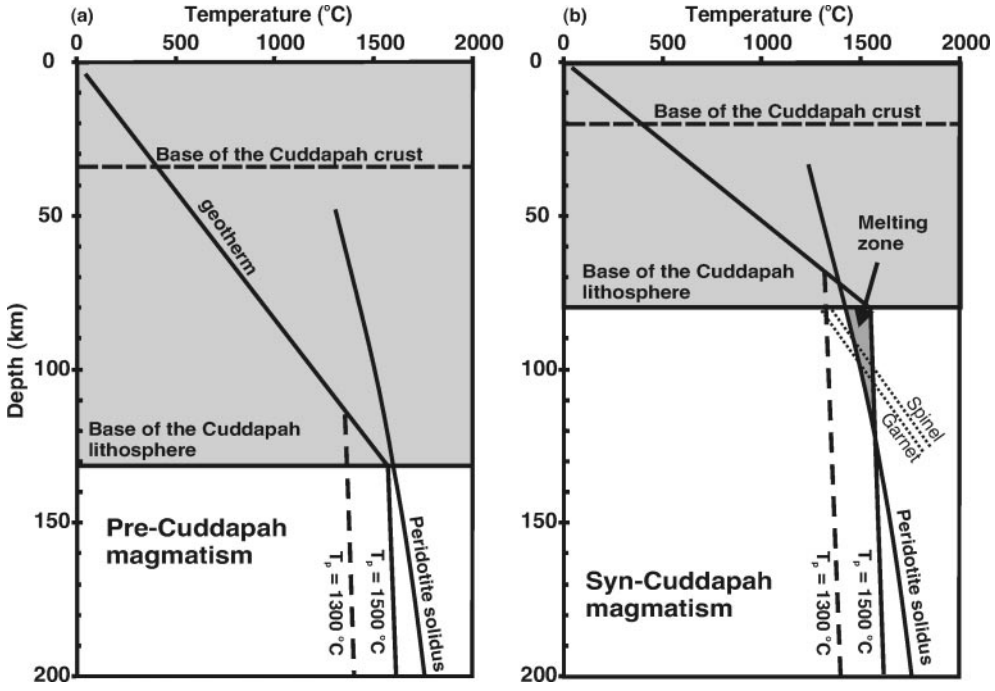

Fig. 17. Model illustrating properties of the lithosphere during (a) pre- and (b) syn-magmatic events in the Cuddapah Basin. The horizontal continuous and dashed lines correspond to the base of the lithosphere and crust, respectively. The position of the geotherm for potential temperatures of 1300°C and 1500°C is shown by dashed and continuous lines. The bold continuous curve is the fertile peridotite solidus (Herzberg *et al.*, 2000).

cases Sr, and in some cases Nb, is systematically depleted in the Cuddapah samples and this possibly indicates the limitation of the REE inversion technique in successfully modelling all of the trace-element concentrations in mafic igneous rocks.

The REE inversion modelling also provides an estimate of the thickness of basaltic melt generated during adiabatic decompression melting and lithospheric extension. For the Cuddapah lavas and sills, the estimated total melt thickness is ~4–5 km. McKenzie & Bickle (1988) calculated the total melt thickness generated by various amounts of lithospheric extension (β) for a given mantle potential temperature and initial MBL thickness. In the case of the Cuddapah lavas and sills, a β factor of 1·6–1·8 is estimated for a mantle potential temperature of 1500°C and an initial MBL thickness of ~120 km. The estimate of the β factor from the REE inversion modelling is in overall agreement with the independent results obtained from subsidence modelling (Anand *et al.*, 2000).

Figure 17 illustrates the postulated geothermal gradient beneath the Cuddapah Basin before and during the magmatic event. Both pre- and syn-magmatic lithospheric and crustal thicknesses are also shown. A maximum initial lithospheric thickness of 132 km at a T_p of ~1450 ± 50°C has been estimated from forward subsidence analyses (Anand *et al.*, 2000) and the forward major- and trace-element modelling. This lithospheric thickness corresponds to an initial MBL thickness of ~120 km. A minimum thickness of ~70 km for the top of the melting column (i.e. the base of the MBL after stretching) has been estimated from the REE inversion modelling. This covers the maximum range of the melting interval predicted by both forward and inverse geochemical modelling.

Comparison with other Proterozoic mafic magmas

The number of worldwide Proterozoic mafic igneous provinces is small and detailed petrological studies have been undertaken in only a few cases. These include the ~2 Ga mafic–ultramafic lava and Konchozero sill complex of the Onega plateau, Baltic shield (Puchtel *et al.*, 1998, 1999) and the ~1·6 Ga mafic volcanic province of the Azul region of the Rio de La Plata craton, central–eastern Argentina (Iacumin *et al.*, 2001). We have inverted the REE abundances of samples from these igneous provinces, as well as samples from Deccan continental flood basalt (CFB), to obtain the melt-fraction distribution curves (Fig. 18). Detailed assessment of lithospheric contamination is not possible for either of these because of the limited published dataset for rocks that may represent crustal and lithospheric end-members. In addition, the depth of the top of the melting column (i.e. the post-magmatic

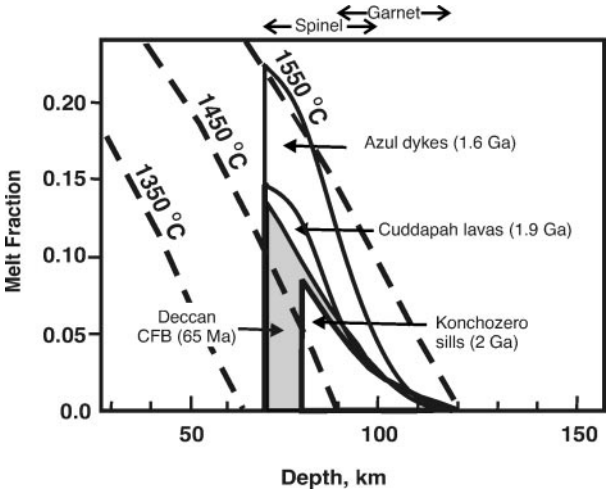

Fig. 18. Melt-fraction distribution curves obtained from inversion modelling of the REE abundances of Konchozero sill and Azul tholeiitic dykes. Representative melt-fraction distribution curves for the Cuddapah and Deccan lavas are also shown for comparison. Cuddapah data are from this work and Deccan data are from Gibson *et al*. (2000).

lithospheric thickness), in each case, was chosen such that it provides the best fit to the REE data. Nevertheless, in both cases, the predicted melt-fraction distribution curve follows a mantle adiabat of ~1500°C, comparable with that of Cuddapah lavas (Fig. 18) and also the Deccan CFB.

Detailed geochemical studies of many other Proterozoic igneous provinces—such as the ~1·1 Ga Keweenawan mid-continent rift system of North America (Hutchinson *et al*., 1990), the 1·26 Ga Mackenzie dykes of NW Canada (LeCheminant & Heaman, 1989) and the 2·39 Ga Scourie dyke swarm of NW Scotland (Weaver & Tarney, 1981)—hold much potential for establishing a comparative tectonomagmatic evolutionary history of these regions and in turn gaining some insight into the Proterozoic evolutionary history of the Earth.

Based on the parameterization of heat flux of the convecting mantle with respect to the average temperature of the convecting layer and its material properties, Richter (1988) proposed a secular cooling curve for the adiabatic temperature of the Earth's interior. This cooling curve predicts that the adiabatic temperature of the Earth at the time when the initiation of the Cuddapah Basin took place (2·0 Ga), is ~1500°C, i.e. 200°C higher than at the present day (Fig. 19). The high mantle potential temperatures predicted for the Archaean are consistent with mantle and crust Sm/Nd ratios, which indicate that the Archaean was a period of very rapid recycling of continental material compared with the Proterozoic and younger times. This may be explained by the considerable change in the thermal regime of the Earth at the Archaean–Proterozoic boundary, which was related to the secular cooling of the Earth and greater preservation of the continental crust. Arndt (1999) has argued that many of the Archaean and Early Proterozoic greenstone belts contain volcanic rocks that erupted subaqueously but interacted with continental crust on their way to the surface. To explain the situation requires that sea levels were high during periods of flood volcanism, perhaps because the ocean basins were partially filled by extensive, active and high-standing ridges or by oceanic plateaux. This is consistent with the secular cooling model of the Earth, which requires expulsion of greater amounts of heat from the mantle during Precambrian times, causing vigorous mantle convection resulting in more active mid-ocean ridges and thicker oceanic crust.

SUMMARY

An attempt has been made to understand the source characteristics and the mantle melting processes that gave rise to the Early Proterozoic (1·9 Ga) lavas and sills of the Cuddapah Basin, southern India. Variations in major-, trace- and rare earth element concentrations of the mafic–ultramafic sills from the Tadpatri Formation highlight the role of crystal fractionation and accumulation in their evolution. Their parental melt compositions appear to have been modified by crystal fractionation in a magma chamber near the base of the crust. In contrast, the Vempalle Fm lavas appear to have been derived from melts that have undergone crystal fractionation at intermediate crustal depths. The maximum Fo content (~85%) of olivines from the Tadpatri sill samples has been used to calculate the Mg number and MgO contents (10 wt %) of their parental melt. This MgO value has subsequently been used to normalize major-element concentrations, by linear regression analysis, to remove the effects of low-pressure fractionation and accumulation.

Trace-element and isotopic ratios have been used to investigate the melt-source characteristics of the Cuddapah lavas and sills. These indicate variable contamination of their parental magma by continental crust. Mixing curves, calculated to model the extent of contamination in the Cuddapah Basin mafic magmas, indicate assimilation of ~10–20% of continental crust during their formation. The sills show larger degrees of crustal contamination than the lavas.

Forward major- and trace-element modelling using Fe and Nd contents of the Cuddapah lavas and sills suggests that they were generated by moderate degrees of partial melting (10–15%) at a mantle potential temperature of ~1500°C. The initial pressures at which the convecting mantle started melting varied from 35 to 40 kbar whereas the top of the melting column was at 27–30 kbar. These results are consistent with those

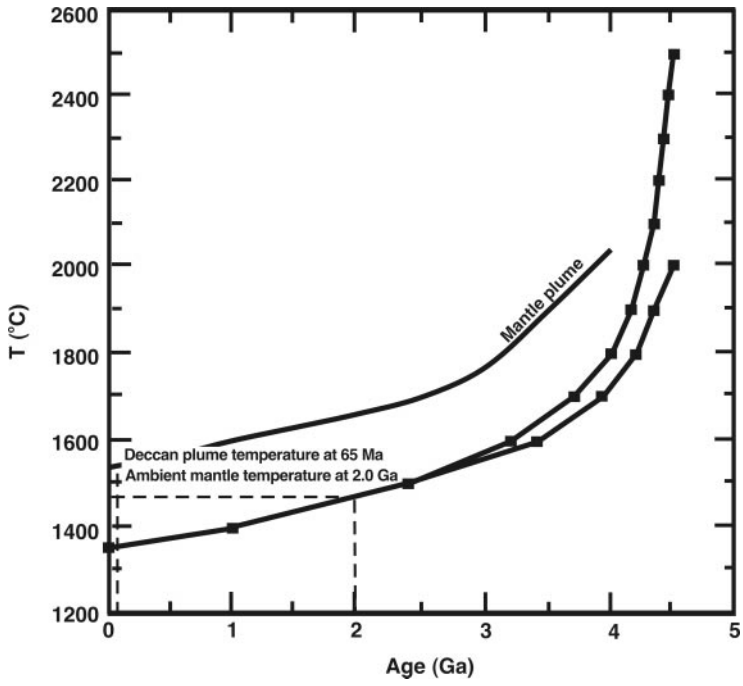

Fig. 19. The predicted secular cooling curves of the average upper-mantle adiabatic temperature (potential temperature, T_p) that can account for the present rate of heat loss from the Earth (Richter, 1988). At 2·0 Ga, the upper-mantle potential temperature was around ~1500°C as shown by dotted lines. The two thermal histories differ only in their assumed initial temperature at 4·5 Ga. The mantle plume curve is from Herzberg (1995).

obtained by REE inversion, which successfully models the observed REE concentrations in the Cuddapah mafic igneous rocks by assimilating 10–15% of 'local' continental crust. The REE inversion model also predicts a depth for the top of the melting column (70 km) that is similar to, but slightly shallower than that obtained by forward major- and trace-element modelling (~80 km). This may be due to the omission of crustal contamination in the forward modelling technique. The melt-fraction distribution curves predicted by the REE inversion modelling follow a mantle adiabat of ~1500°C, which is consistent with the forward major- and trace-element modelling and the secular cooling model of the Earth (Richter, 1988; Fig. 19). A β factor of 1·6–1·8 is estimated from the thickness of basaltic melt (>4 km) generated below the Cuddapah Basin at a mantle potential temperature of ~1500°C. This result is in overall agreement with β factor estimates obtained by subsidence modelling (Anand *et al.*, 2000). The high mantle potential temperatures below the Cuddapah Basin at ~2·0 Ga, predicted by the geochemical modelling, are consistent with the secular cooling model of the Earth (Turcotte, 1980; Richter, 1988) and do not require the presence of a mantle plume below the southeastern Dharwar Craton at ~2·0 Ga. Lithospheric extension and intra-cratonic basin formation appears to be the result of passive rather than active rifting processes.

ACKNOWLEDGEMENTS

Stephen Reed and Ron Hardy are thanked for assistance with electron microprobe and XRF analyses, respectively. Jo Greenwood, Kym Jarvis and Jon Williams are also acknowledged for their help with ICP-MS analyses at the NERC facility, Kingston University, Surrey. Nicky White, Nagaraja Rao, various colleagues from the Geological Survey of India, and Dr Kumar Eswaran and his family are thanked for their help in the field-work, sample collection and logistical support. Jon Maclennan and Paula Smith provided stimulating discussions about the REE inversion technique. M.A. thanks the Cambridge Commonwealth Trust and Cambridge Nehru Trust for providing a Ph.D. scholarship, and the Department of Earth Sciences, University of Cambridge, for financial assistance with field and analytical work. This manuscript benefited greatly from the constructive reviews and criticisms by Don Francis, Talat Ahmed, N. V. Chalapathi Rao and Dennis Geist. This is a Department of Earth Sciences, University of Cambridge contribution no. 7474.

REFERENCES

Anand, M. (2001). Tectono-magmatic evolution of the intracratonic Cuddapah Basin, India. Ph.D. thesis, University of Cambridge, 248 pp.

Anand, M., Gibson, S. A., White, N. J. & Kelley, S. P. (2000). Mafic magmatism and subsidence history of the intra-cratonic Proterozoic Cuddapah Basin, Southern India (abstract). *American Geophysical Union Fall Meeting. EOS Transactions, American Geophysical Union* **81**(48), F1363.

Arndt, N. (1999). Why was flood volcanism on submerged continental platforms so common in the Precambrian? *Precambrian Research* **97**, 155–164.

Aswathanarayana, U. (1962*a*). Age of the Cuddapahs, India. *Nature* **163**, 470.

Aswathanarayana, U. (1962*b*). Age of the Cuddapahs, India. *Nature* **194**, 566.

Bhaskar Rao, Y. J., Pantulu, G. V. C., Reddy, V. D. & Gopalan, K. (1995). Time of early sedimentation and volcanism in the Proterozoic Cuddapah basin, South India: evidence from the Rb–Sr age of Pulivendla mafic sill. In: Devaraju, T. C. (ed.) *Dyke Swarms of Peninsular India. Memoir of the Geological Society of India* **33**, 329–338.

Bickle, M. J. & Eriksson, K. A. (1982). Evolution and subsidence of Early Precambrian sedimentary basins. *Philosophical Transactions of the Royal Society of London, Series A* **305**, 225–247.

Chalapathi Rao, N. V. (1997). Petrogenesis of the Proterozoic kimberlites and lamproites from the Cuddapah Basin and Dharwar craton, southern India. Ph.D. thesis, University of Cambridge.

Chalapathi Rao, N. V., Miller, J. A., Pyle, D. M. & Madhavan, V. (1996). New Proterozoic K–Ar ages for some kimberlites and lamproites from the Cuddapah basin and Dharwar craton, South India: evidence for non-contemporaneous emplacement. *Precambrian Research* **79**, 363–369.

Chalapathi Rao, N. V., Gibson, S. A., Pyle, D. M. & Dickin, A. P. (1998). Contrasting isotopic mantle sources for Proterozoic lamproites and kimberlites from the Cuddapah Basin and Eastern Dharwar Craton: implication for Proterozoic mantle heterogeneity beneath southern India. *Journal of the Geological Society of India* **52**, 683–694.

Chalapathi Rao, N. V., Miller, J. A., Gibson, S. A., Pyle, D. M. & Madhavan, V. (1999). Precise ^{40}Ar–^{39}Ar age determinations of the Kotakonda kimberlite and Chelima lamproite, India: implication to the timing of mafic dyke swarm emplacement in the Eastern Dharwar Craton. *Journal of the Geological Society of India* **53**, 425–432.

Chatterjee, N. & Bhattacharji, S. (1998). Formation of Proterozoic tholeiite intrusives in and around Cuddapah Basin, South India and their Gondwana counterparts in East Antarctica; and compositional variation in their mantle sources. *Neues Jahrbuch für Mineralogie, Abhandlungen* **174**, 79–102.

Chaudhuri, A. K., Saha, D., Deb, G. K., Deb, S. P., Mukherjee, M. K. & Ghosh, G. (2002). The Purana basins of southern cratonic province of India—a case for Mesoproterozoic fossil rifts. *Gondwana Research* **5**, 22–33.

Crawford, A. R. & Compston, W. (1973). The age of the Cuddapah and Kurnool systems, Southern India. *Journal of the Geological Society of Australia* **19**, 453–464.

Deer, W. A., Howie, R. A. & Zussman, J. (1992). *An Introduction to the Rock-forming Minerals*. Harlow: Longman, 695 pp.

Gibson, S. A., Thompson, R. N., Leonardos, D. H., Dickin, A. P. & Mitchell, J. G. (1995). The Late Cretaceous impact of the Trindade mantle plume—evidence from large-volume, mafic, potassic magmatism in SE Brazil. *Journal of Petrology* **36**, 189–229.

Gibson, S. A., Thompson, R. N., Leonardos, O. H., Dickin, A. P. & Mitchell, J. G. (1999). The limited extent of plume–lithosphere interactions during continental flood-basalt genesis: geochemical evidence from Cretaceous magmatism in southern Brazil. *Contributions to Mineralogy and Petrology* **137**, 147–169.

Gibson, S. A., Thompson, R. N. & Dickin, A. P. (2000). Ferropicrites: geochemical evidence for Fe-rich streaks in upwelling mantle plumes. *Earth and Planetary Science Letters* **174**, 355–374.

Goodwin, A. M. (1996). *Principles of Precambrian Geology*. London: Academic Press, 327 pp.

Helz, R. T. (1980). Chemical and experimental study of the Yakima Basalt subgroup: evidence for intercrust storage and contamination (abstract). *EOS Transactions, American Geophysical Union* **61**, 68.

Herzberg, C. (1995). Generation of plume magmas through time: an experimental perspective. *Chemical Geology* **126**, 1–16.

Herzberg, C. & Zhang, J. (1996). Melting experiments on anhydrous peridotite KLB-1: compositions of magmas in the upper mantle and transition zone. *Journal of Geophysical Research* **101**, 8271–8295.

Herzberg, C., Raterron, P. & Zhang, J. (2000). New experimental observations on the anhydrous solidus for peridotite KLB-1. *Geochemistry, Geophysics, Geosystems* **1**, xx.

Hutchinson, D. R., White, R. S., Cannon, W. F. & Schulz, K. J. (1990). Keweenaw Hot Spot: geophysical evidence for a 1·1 Ga mantle plume beneath the Midcontinent Rift System. *Journal of Geophysical Research* **95**, 10869–10884.

Iacumin, M., Piccirillo, E. M., Girardi, V. A. V., Teixeira, W., Bellieni, G., Echeveste, H., Fernandez, J. P. P. & Ribot, A. (2001). Early Proterozoic calc-alkaline and Middle Proterozoic tholeiitic dyke swarms from central–eastern Argentina: petrology, geochemistry, Sr–Nd isotopes and tectonic implications. *Journal of Petrology* **42**, 2109–2143.

Ikramuddin, M. & Stueber, A. M. (1976). Rb–Sr ages of Precambrian dolerite and alkaline dykes, southeast Mysore State, India. *Lithos* **9**, 235–241.

Irvine, T. N. & Baragar, W. R. A. (1971). A guide to the chemical classification of the common volcanic rocks. *Canadian Journal of Earth Sciences* **8**, 523–548.

Klemme, S. & O'Neil, H. S. C. (2000). The near-solidus transition from garnet lherzolite to spinel lherzolite. *Contributions to Mineralogy and Petrology* **138**, 237–248.

Kostopoulos, D. K. & James, S. D. (1992). Parameterization of the melting regime of the shallow upper mantle and the effects of variable lithospheric stretching on mantle model stratification and trace-element concentrations in magmas. *Journal of Petrology* **33**, 665–691.

Langmuir, C. H., Klein, E. M. & Plank, T. (1992). Petrological systematics of mid-ocean ridge basalts: constraints on melt generation beneath ocean ridges. In: Phipps-Morgan, J., Blackman, D. K. & Sinton, J. (eds) *Mantle Flow and Melt Generation at Mid-Ocean Ridges. Geophysical Monograph, American Geophysical Union* **71**, 183–280.

LeCheminant, A. N. & Heaman, L. M. (1989). Mackenzie igneous events, Canada: Middle Proterozoic hotspot magmatism associated with ocean opening. *Earth and Planetary Science Letters* **96**, 38–48.

Le Maitre, R. W. (2002). *Igneous Rocks: a Classification and Glossary of Terms: Recommendations of the International Union of Geological Sciences Subcommission on the Systematics of Igneous Rocks*. Cambridge: Cambridge University Press, 236 pp.

McKenzie, D. (1989). Some remarks on the movement of small melt fractions in the mantle. *Earth and Planetary Science Letters* **95**, 53–72.

McKenzie, D. & Bickle, M. J. (1988). The volume and composition of melt generated by extension of the lithosphere. *Journal of Petrology* **29**, 625–679.

McKenzie, D. & O'Nions, R. K. (1991). Partial melt distributions from inversion of rare earth element concentrations. *Journal of Petrology* **32**, 1021–1091.

McKenzie, D. & O'Nions, R. K. (1998). Melt production beneath oceanic islands. *Physics of the Earth and Planetary Interiors* **107**, 143–182.

McKenzie, D. P., Nisbet, E. & Sclater, J. G. (1980). Sedimentary basin development in the Archean. *Earth and Planetary Science Letters* **48**, 35–41.

Mishra, D. C. & Tiwari, V. M. (1995). An asymmetrical basic lopolith below sediments in western Cuddapah Basin—geophysical evidence. *Tirupati 1995, Annual Convention of the Geological Society of India. Geological Society of India, Special Volume* 31–41.

Murthy, Y. G. K., Rao, V. B., Guptasarma, D., Rao, J. M., Rao, M. N. & Bhattacharji, S. (1987). Tectonic, petrochemical and geophysical studies of mafic dyke swarms around the Proterozoic Cuddapah basin, South India. *Geological Association of Canada, Special Papers* **34**, 303–316.

Nagaraja Rao, B. K. & Ramalingaswamy, G. (1976). Some new thoughts on the stratigraphy of Cuddapah Supergroup. *Seminar on Kaladgi–Badami, Bhima and Cuddapah Supergroup*. Mysore, India, pp. 17–20.

Nakamura, N. (1974). Determination of REE, Ba, Fe, Mg, Na and K in carbonaceous and ordinary chondrites. *Geochimica et Cosmochimica Acta* **38**, 757–775.

O'Nions, R. K. (1992). *The Continents*. Cambridge: Cambridge University Press, pp. 145–164.

Puchtel, I. S., Arndt, N. T., Hofmann, A. W., Hasse, K. M., Kröner, A., Kulikov, V. S., Kulikova, V. V., Garbe-Schönberg, C.-D. & Nemchin, A. A. (1998). Petrology of mafic lavas within the Onega plateau, central Karelia: evidence for 2·0 Ga plume-related continental crustal growth in the Baltic shield. *Contributions to Mineralogy and Petrology* **130**, 134–153.

Puchtel, I. S., Brügmann, G. E. & Hofmann, A. W. (1999). Precise Re–Os mineral isochron and Pb–Nd–Os isotopic systematics of a mafic–ultramafic sill in the 2·0 Ga Onega plateau (Baltic shield). *Earth and Planetary Science Letters* **170**, 447–461.

Rao, M., Bhattacharji, S., Rao, M. N. & Hermes, O. D. (1995). Ar–Ar ages and geochemical characteristics of dolerite dykes around the Proterozoic Cuddapah basin, South India. In: Devaraju, T. C. (ed.) *Dyke Swarms of Peninsular India. Geological Society of India. Memoir of the Geological Society of India* **33**, 307–328.

Richter, F. M. (1988). A major change in the thermal state of the Earth at the Archean–Proterozoic boundary: consequences for the nature and preservation of continental lithosphere. *Journal of Petrology, special lithosphere volume* 39–52.

Rollinson, H. (1993). *Using Geochemical Data: Evaluation, Presentation, Interpretation*. Harlow: Longman.

Roy, A. K. (1947). Geology of the Dhone taluk and neighbouring parts, Kurnool districts. Unpublished Geological Survey of India Progress Report (1945–1946).

Taylor, S. R. & McLennan, S. M. (1981). The composition and evolution of the continental crust: rare-earth element evidence from sedimentary rocks. *Philosophical Transactions of the Royal Society of London, Series A* **301**, 381–399.

Thompson, R. N., Dickin, A. P., Gibson, I. L. & Morrison, M. A. (1982). Elemental fingerprints of isotopic contamination of Hebridean Palaeocene mantle-derived magmas by Archean sial. *Contributions to Mineralogy and Petrology* **79**, 159–168.

Thompson, R. N., Morrison, M. A., Dickin, A. P. & Hendry, C. L. (1983). *Continental Flood Basalts ... Arachnids Rule OK?* Nantwich: Shiva, pp. 158–185.

Thompson, R. N., Morrison, M. A., Hendry, G. L. & Parry, S. J. (1984). An assessment of the relative roles of crust and mantle in magma genesis: an elemental approach. *Philosophical Transactions of the Royal Society of London, Series A* **310**, 549–590.

Turcotte, D. L. (1980). On the thermal evolution of the Earth. *Earth and Planetary Science Letters* **48**, 53–58.

Ulmer, P. (1989). The dependence of the Fe^{2+}–Mg cation-partitioning between olivine and basaltic liquid on pressure, temperature and composition, an experimental study to 30 kbars. *Contributions to Mineralogy and Petrology* **101**, 261–273.

Vijayam, E. (1968). An interesting dyke near Archean–Cuddapah boundary, Veldurti, Kurnool District, Andhra Pradesh. *Current Science* **37**, 15.

Wakita, H., Rey, P. & Schmitt, R. A. (1971). Abundances of the 14 rare-earth elements and 12 other trace elements in Apollo 12 samples: five igneous and one breccia rocks and four soils. *Proceedings of the 2nd Lunar Science Conference. Geochimica et Cosmochimica Acta Supplement 2*, 1319–1329.

Weaver, B. L. & Tarney, J. (1981). The Scourie dyke suite: petrogenesis and geochemical nature of the Proterozoic sub-continental mantle. *Contributions to Mineralogy and Petrology* **78**, 175–188.

Weaver, B. L. & Tarney, J. (1984). Empirical approach to estimating the composition of the continental crust. *Nature* **310**, 575–577.

Zachariah, J. K., Bhaskar Rao, Y. J., Srinivasan, R. & Gopalan, K. (1999). Pb, Sr and Nd isotope systematics of uranium mineralized stromatolitic dolomites from the Proterozoic Cuddapah Supergroup, south India: constraints on age and provenance. *Chemical Geology* **162**, 49–64.